AFRL-RY-WP-TR-2014-0144

DYNAMICS-ENABLED NANOELECTROMECHANICAL SYSTEMS (NEMS) OSCILLATORS

Michael Roukes

California Institute of Technology
Kavli Nanoscience Institute

Mark Dykman

Michigan State University

JUNE 2014
Final Report

AIR FORCE RESEARCH LABORATORY
SENSORS DIRECTORATE
WRIGHT-PATTERSON AIR FORCE BASE, OH 45433-7320
AIR FORCE MATERIEL COMMAND
UNITED STATES AIR FORCE

NOTICE AND SIGNATURE PAGE

Using Government drawings, specifications, or other data included in this document for any purpose other than Government procurement does not in any way obligate the U.S. Government. The fact that the Government formulated or supplied the drawings, specifications, or other data does not license the holder or any other person or corporation; or convey any rights or permission to manufacture, use, or sell any patented invention that may relate to them.

This report is the result of contracted fundamental research deemed exempt from public affairs security and policy review in accordance with SAF/AQR memorandum dated 10 Dec 08 and AFRL/CA policy clarification memorandum dated 16 Jan 09. This report is available to the general public, including foreign nationals.

AFRL-RY-WP-TR-2014-0144 HAS BEEN REVIEWED AND IS APPROVED FOR PUBLICATION IN ACCORDANCE WITH ASSIGNED DISTRIBUTION STATEMENT.

*//Signature//

SARAH B. DOOLEY, Program Manager
Optoelectronics Technology Branch
Aerospace Components & Subsystems Division

//Signature//

JONAHIRA R. ARNOLD, Chief
Optoelectronics Technology Branch
Aerospace Components & Subsystems Division

*//Signature//

BRADLEY D. CHRISTIANSEN, USAF, Lt Col
Deputy Division Chief
Aerospace Components & Subsystems Division
Sensors Directorate

This report is published in the interest of scientific and technical information exchange, and its publication does not constitute the Government's approval or disapproval of its ideas or findings.

*Disseminated copies will show "//signature//" stamped or typed above the signature blocks.

REPORT DOCUMENTATION PAGE

Form Approved
OMB No. 0704-0188

1. REPORT DATE *(DD-MM-YY)*	2. REPORT TYPE	3. DATES COVERED *(From - To)*
June 2014	Final	14 June 2010 – 11 December 2013

4. TITLE AND SUBTITLE
DYNAMICS-ENABLED NANOELECTROMECHANICAL SYSTEMS (NEMS) OSCILLATORS

5a. CONTRACT NUMBER
FA8650-10-1-7029

5b. GRANT NUMBER

5c. PROGRAM ELEMENT NUMBER
61101E

6. AUTHOR(S)
Michael Roukes (California Institute of Technology, Kavli Nanoscience Institute)
Mark Dykman (Michigan State University)

5d. PROJECT NUMBER
1000

5e. TASK NUMBER
YD

5f. WORK UNIT NUMBER
Y0G9

7. PERFORMING ORGANIZATION NAME(S) AND ADDRESS(ES)
California Institute of Technology
Kavli Nanoscience Institute
114-36
Pasadena, CA 91125

Michigan State University
East Lansing, MI 48823

8. PERFORMING ORGANIZATION REPORT NUMBER
AFRL-RY-WP-TR-2014-0144

9. SPONSORING/MONITORING AGENCY NAME(S) AND ADDRESS(ES)
Air Force Research Laboratory
Sensors Directorate
Wright-Patterson Air Force Base, OH 45433-7320
Air Force Materiel Command
United States Air Force

Defense Advanced Research Projects Agency
DARPA/MTO
675 North Randolph Street
Arlington, VA 22203-2114

10. SPONSORING/MONITORING AGENCY ACRONYM(S)
AFRL/RYDH

11. SPONSORING/MONITORING AGENCY REPORT NUMBER(S)
AFRL-RY-WP-TR-2014-0144

12. DISTRIBUTION/AVAILABILITY STATEMENT
Approved for public release; distribution unlimited

13. SUPPLEMENTARY NOTES
This report is the result of contracted fundamental research deemed exempt from public affairs security and policy review in accordance with SAF/AQR memorandum dated 10 Dec 08 and AFRL/CA policy clarification memorandum dated 16 Jan 09. This material is based on research sponsored by Air Force Research Laboratory (AFRL) and the Defense Advanced Research Agency (DARPA) under agreement number FA8650-10-1-7029. The U.S. Government is authorized to reproduce and distribute reprints for Governmental purposes notwithstanding any copyright notation thereon. The views and conclusions contained herein are those of the authors and should not be interpreted as necessarily representing the official policies or endorsements, either expressed or implied, of AFRL and DARPA or the U.S. Government. Report contains color

14. ABSTRACT
The program goal was to develop compact frequency sources capable of maintaining low phase noise under high accelerations or vibrations and over a wide temperature range. The effort strived to better understand, engineer, and demonstrate nonlinear-dynamics-enabled nanoelectromechanical system (NEMS) frequency-source technology.

15. SUBJECT TERMS
Oscillator, phase noise, nanomembrane, nanoelectromechanical system

16. SECURITY CLASSIFICATION OF:			17. LIMITATION OF ABSTRACT:	18. NUMBER OF PAGES	19a. NAME OF RESPONSIBLE PERSON (Monitor)
a. REPORT	b. ABSTRACT	c. THIS PAGE			Sarah Dooley
Unclassified	Unclassified	Unclassified	SAR	58	19b. TELEPHONE NUMBER *(Include Area Code)* N/A

Table of Contents

Section **Page**

Section **Page**

List of Figures

Figure **Page**

Figure **Page**

Figure **Page**

List of Tables

Table **Page**

1.0 SUMMARY AND HIGHLIGHTS

A self-sustained oscillator is a crucial element for a wide range of applications that includes reference clocks for electronics, radar technologies, and precision timekeeping. Although oscillator technology has existed for several millennia, the conceptual building blocks have remained the same for many centuries. The overarching goal of the Dynamic Enabled Frequency Sources (DEFYS) program is to reassess traditional perspectives about oscillator architectures and their limitations. The stated the major objectives of the program are:

- Objective 1 – "*Use nonlinearity to reduce phase noise"*
- Objective 2 – *"Tune the system to optimize performance for a given noise level"*
- Objective 3 – *"Innovative engineering"*

As delineated below, our Program effort successfully addressed all of these program objectives. In particular, our work on using nonlinearity to reduce phase noise was the singular success of the DEFYS program. **We are the sole group to provide both the theoretical underpinning and experimental demonstrations of the use of <u>nonlinear mechanical response</u> – *which occurs on the timescale of the natural dynamics of the system* – to suppress phase noise.** By contrast, nonlinearity arising from processes other than the mechanical dynamics, such as thermal heating, will typically affect processes only on much slower timescales.

1.1 Objective 1 – "Use Nonlinearity to Reduce Phase Noise"

We carried out extensive theoretical work to investigate the dynamics of an oscillator based on a nonlinear-frequency-determining element and its feedback loop, and our approach considered these together as a complete system. We developed a universal model for the effects of important noise processes on the oscillator phase noise. Figure 1 schematically depicts our perspective on the problem (see Appendix B.2 for a theoretical survey). Careful analysis of each process, shown as an arrow in the figure, has led us to develop innovative oscillator architectures and establish novel operating conditions that optimize the system phase noise characteristics. We successfully conceived of and implemented techniques that simultaneously eliminated noise in feedback phase Δ, minimized noise in saturation, and suppressed amplitude dependent noise mechanisms (the four rightmost arrows in Figure 1) by operating in the vicinity of the second instability point of a Duffing oscillator. This will be described below. Further, we explored a wide range of input parameters and observed ~10 dBc/Hz phase noise reduction (compared to optimized linear oscillator) at what we term a "Kenig point".

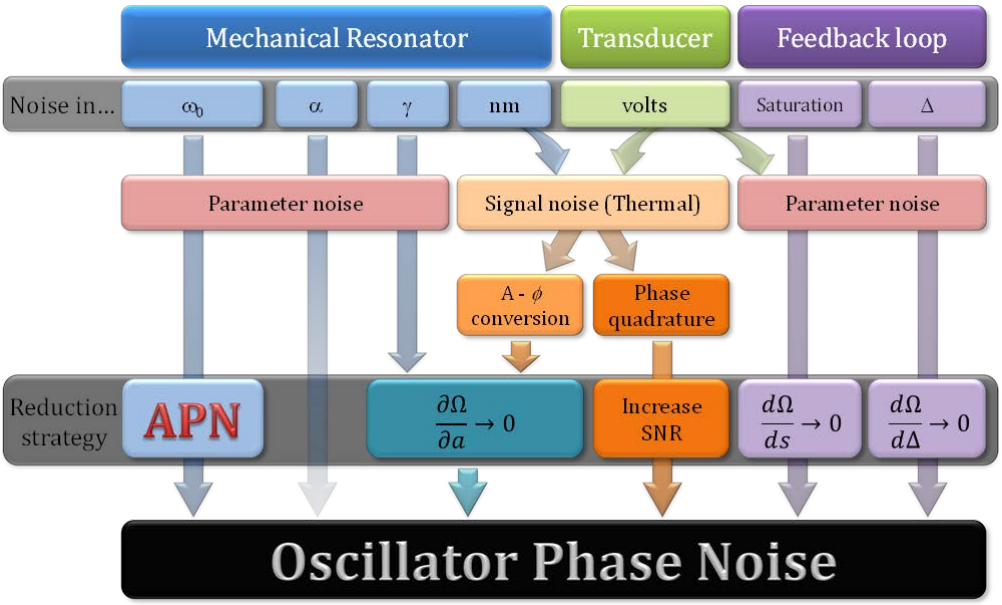

Figure 1: Roadmap for improving the Noise of Nanoelectromechanical System (NEMS) Based Oscillators

Part of the noise is internal, arising from the resonator itself, as fluctuations of the natural frequency (ω_0), nonlinear stiffness (α), dissipation (γ), or due to thermomechanical noise causing Brownian motion of the resonator (nm). Noise also originates from the feedback loop, which includes the transducer and the amplifier, and manifests as noise in the electrical signal (volts), in the saturation of the feedback signal (s), and in the loop phase-shift (Δ). The map indicates methods for suppressing the oscillator phase noise. Ω denotes oscillator frequency and APN is shorthand for Anomalous Phase Noise, which will be described later in the text.

1.2 Objective 2 – "Tune the System to Optimize Performance for a Given Noise Level"

Theoretical analysis predicts that the coupling between amplitude and frequency present in nonlinear oscillators (light orange box in Figure 1) is equivalent to an additional phase noise source (represented as the blue arrow at the bottom of Figure 1.) However, if the nonlinearity of the system is tuned so that amplitude/frequency coupling dependence, which we term the "backbone", possesses an extremum, then at this point this noise source can be eliminated. We discovered methods to control the nonlinear properties of our devices, and demonstrated backbone curves with these extremal "sweet spots". We implemented backbone control in nonlinear NEMS oscillators, and utilized extremal operating points to obtain ~10dBc/Hz phase noise reduction (see Appendix A.3-(b) for details).

We complemented this work on backbone control by novel studies that are especially important for creating oscillators from nanoscale resonators. Specifically, we generalized the concept of an oscillator by implementing a strongly nonlinear feedback function proportional to the square of the signal applied to a resonator's parametric input. The innovative architecture permits realization of steady oscillator circuits while circumventing the need to satisfy the Barkhausen criterion, which is often impossible to achieve for nanoscale systems possessing electromechanical impedances profoundly ill-matched to electronic circuit impedances. Our new paradigm therefore enables oscillator development with a previously unattainable and wide variety of nanoscale devices. We observed phase noise reduction of ~25 dBc/Hz compared to the performance of an optimized linear oscillator. We further demonstrated scalability of the concept and its potential for a wide range of

applicability by implementing it at high frequency on a compact printed circuit board in collaboration with our industrial partner Rockwell Collins (see Appendix A.4 for details).

1.3 Objective 3 – "Innovative Engineering"

In this Program, we have made important advances in the engineering oscillators based on nanoscale mechanical-frequency-determining elements, following the original DEFYS program announcement guidelines: *"meeting the goals of DEFYS will require an alternative architecture using a nanoscale oscillator"*. We invented novel transduction technologies based on nanoscale piezoelectric actuation and piezometallic detection, applicable in a wide range of geometries (see Appendix A.2). The remarkable sensitivity of the technique allowed the measurement of the intrinsic thermomechanical noise of NEMS resonators. We characterized the nonlinear properties of doubly-clamped beam NEMS resonators, and have confirmed the validity of Euler-Bernoulli theory for the first three vibrational modes and their intermodal nonlinear coupling strengths (see Appendix A.2-(a)). By developing a clever background reduction technique, we were also able to demonstrate the highest reported frequency room temperature NEMS feedback oscillator to date, operating at 180 MHz (see Appendix A.3-(a)). The flexibility and high level of control of these NEMS resonators have since enabled a variety of experiments that employ nonlinearity to improve phase noise (described below).

2.0 FUNDAMENTAL ACHIEVEMENTS

2.1 Nonlinear Dynamics Enhancement of Phase Noise Performance

The Caltech/ Michigan State University (MSU) program is unique among those of DEFYS performers in its aggressive focus on NEMS. The central purpose of the Caltech/MSU DEFYS program, as originally envisioned and proposed, is to pursue opportunities for optimizing phase noise performance beyond that available in the linear operating regime of NEMS resonators. At the outset, salient facts were known about NEMS from our work for frequency control and sensing applications. As the size of a flexural NEMS resonator is scaled downward:

- it becomes strongly nonlinear, and thus constitutes an archetypal candidate for nonlinear engineering
- its fundamental resonant frequency scales upward into the ultra-high frequency (UHF) and microwave bands, thus providing ready access to nonstandard domains for quartz frequency control devices
- its linear dynamic range decreases precipitously, posing a challenge for low phase noise operation

Given these considerations, we realized that to achieve the Phase I metrics with a NEMS flexural resonator, specifically – creating a 500 megahertz (MHz) oscillator with phase noise performance of -90dBc at 1 kilohertz (KHz) offset – would require at least a 10 decibel (dB) improvement in the operating dynamic range of the device. This is depicted in Figure 2.

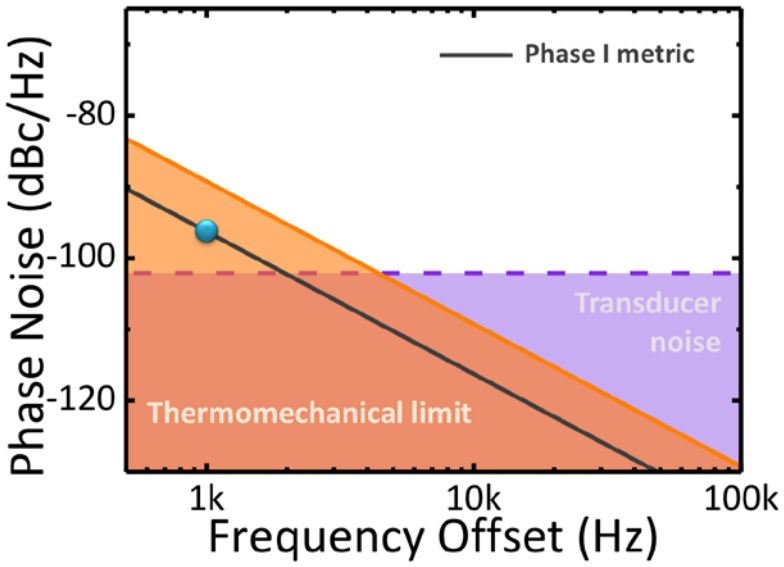

Figure 2: Phase Noise Performance Achievable with a Conventional Linear Oscillator using a NEMS Doubly Clamped Beam

We assume the main limiting physical mechanisms are thermomechanical noise (orange) and transducer noise typical for piezometallic detection (purple). The blue point marker shows the DEFYS Phase I metric. The grey line represents the expected phase noise dependence for an oscillator meeting DEFYS milestone, which typically scales as $(\Delta f)^{-2}$*. This estimation depicts the 10dB difference between the originally anticipated NEMS oscillator performance and the DEFYS Phase I goal. Our original proposal outlined techniques utilizing nonlinear dynamics by which we intended to reduce phase noise by 10 to 20 dB and thus meet the Phase I metric.*

Our effort's stated Phase I program goal was to employ nonlinear dynamics to achieve this requisite 10 dB improvement to meet the Phase I metric. In this report we describe our success at:

- Theoretically identifying several entirely new mechanisms that employ nonlinear dynamics in NEMS-based oscillators to achieve phase noise improvements beyond the linear operating regime.
- Experimentally demonstrating concrete implementations of these new mechanisms in NEMS oscillators to provide 10-20dB performance enhancement from nonlinear dynamics.

2.2 Identification of Generic, Anomalous Phase Noise

In the course of our work we made an important and unexpected discovery – one, however, that has proven deleterious to the absolute phase noise performance achieved so far. We find, quite generally, that the noise floor of a nanomechanical resonator is not simply determined by thermomechanical fluctuations when it is driven into the nonlinear regime. **This is a pivotal finding, and motivates a critical reassessment of the initial founding assumptions of the DEFYS program.** This is critical, because initial assumptions about the attendant improvements available from dynamical enhancements in the nonlinear regime implicitly assumed that the noise floor could be improved by operating in that regime if amplitude to frequency noise conversion could be addressed. Our findings prove otherwise; we have found stable "sweet spots" where such noise conversion is completely suppressed, *but where additional frequency/phase noise* – beyond that expected from thermomechanical fluctuations – *becomes dominant.* This noise arises either from the activated processes in the driven regime (through mechanisms akin to 1/f noise in the electrical domain), or from other as-yet-unknown intrinsic frequency-fluctuation processes. This is clearly depicted for operation at what we term a Kenig point of a Duffing oscillator, as shown in Figure 3. The experimental data and our analysis provide very strong evidence that we have a firm understanding of the principal sources of noise in our system. Together they illustrates the importance for tackling, that is, understanding and suppressing, anomalous phase noise (APN) to achieve optimized performance in NEMS oscillators. (Further discussion is provided in Appendix A.3-(d)). Accordingly, the next part of this quest is to understand: i) how general are these noise phenomena, ii) what microscopic mechanisms are at the origin of such "anomalous phase noise", and iii) what steps can be taken to ameliorate it. We have begun this work in the latter months of Phase I and during Phase IB, and plan to continue it in our future research.

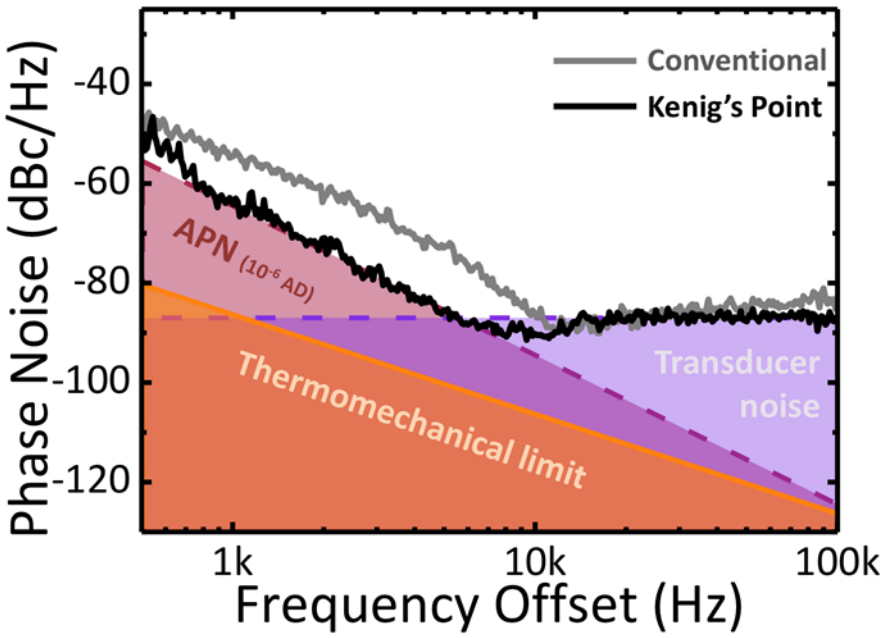

Figure 3: Achieved Phase Noise Performance Improvement for a 15MHz Flexural NEMS-Based Oscillator Operating at its "Kenig Point"

The gray trace depicts experimental data from a conventional oscillator architecture. The black trace represents oscillator operation biased at the "Kenig point" in the nonlinear regime. Improvement of 10 dB is achieved. The pink region shows the estimated APN contribution, which is deduced from measured Allan Deviation (AD) values, ~10^{-6}. The purple region depicts transducer noise, estimated from the measured system noise level. The orange region shows phase noise originating from thermomechanical noise, which, in our proposal, we originally assumed imposed the ultimate limits to phase noise performance. The very close agreement between the black curve (for oscillator operation at the Kenig point) with the pink and purple regions, provides very strong evidence that we have a firm understanding of the principal sources of noise in our system. This illustrates the importance for tackling, that is, understanding and suppressing, APN to achieve optimized performance.

2.3 Caltech MEMS Oscillators

As part of our quest to understand the mechanisms behind anomalous phase noise in driven nanoelectromechanical systems we have also built self-sustained oscillators from microwave frequency *micro*mechanical resonators operating at 2.2 gigahertz (GHz). These devices employed piezoelectric actuation and readout, using bulk Lamb-wave resonances. With these devices, we measured an intrinsic phase noise level of -82 dBc/Hz (at 1 kHz offset, scaled to 1 GHz), quite close to the program metric. Our most recent have in the last several weeks provided excellent devices that we project should have phase noise performance of order -100 dBc/Hz at 1 KHz offset, scaled to 1 GHz, exceeding the DEFYS Phase I program metric (Appendix A.1.).

This project was important for helping us to develop methodologies for very high frequency oscillator measurements, understanding the limitations of our electronic circuits, evaluating the importance of matching and, subsequently, demonstrating low phase noise performance.

2.4 Synchronization-based Improvements in the Presence of Anomalous Phase Noise

Finally, in preliminary exploratory work, we successfully demonstrated synchronization of two nonlinear NEMS-based oscillators. The mechanical devices employed were physically separated, and their interaction was engineered by means of off-the-shelf electronic circuit components. What is important about these preliminary efforts is that we observed expected 3 dB phase noise reduction; this work is described in Appendix A.3-(e). This work clearly demonstrates the potential for easily building large arrays of nonlinear oscillators with electronically engineered coupling, and that the phase noise for synchronized arrays can be reduced by a factor of order the size of the array. The latter holds true, despite limitations from anomalous phase noise. We will return to this important point below.

3.0 FUTURE PLANS

Although much has been achieved within this Program, there remain significant milestones set out by the long-term DEFYS program that are yet to be accomplished. For example, the principal Phase II DEFYS metrics involve creation of a dynamics-enabled NEMS oscillator at 800MHz with phase noise performance at or below -110dBc at 1kHz offset. Although there are other noteworthy metrics, we believe that it is most important for us to address here how we believe our approach can achieve these milestones – especially in light of the anomalous phase noise that our Phase I efforts have unveiled.

We plan three complementary approaches that each, separately, should allow us to significantly improve our frequency/phase-noise metrics. These approaches are: i) directly tackling and, hopefully, suppressing anomalous phase noise by carefully investigating and engineering NEMS devices, ii) use of nanomembrane-based devices that should permit lower phase noise operation than achievable with flexural NEMS resonators, while still permitting nonlinear dynamics enhancement, and, iii) use of array-based synchronization techniques that will permit achieving improved metrics with an ensemble of oscillators.

3.1 Identification and Suppression of Anomalous Phase Noise

To identify the origin of anomalous phase noise we have constructed an apparatus during the latter half this Program that will now allow experimental investigations of phase noise in NEMS resonators beginning from highly controlled conditions. Specifically, the surface preparation of NEMS has never really been carefully studied nor engineered and as device size is scaled downward and the surface-to-volume ratio becomes very significant. Our work (for example, as described in Appendix B.3) highlights the importance of surface phenomena for phase noise processes. The first step in the planned experimental work will be to make careful measurements to understand the origin of the excess noise; the second step will then be to devise engineering approaches to ameliorate this noise as much as possible.

3.2 Development of 1GHz Circular Nanomembrane Oscillators

To achieve nanomechanical resonators with very high natural frequencies (0.8-1 GHz) without making them inconveniently small, device stiffness must be scaled upward. The consequence of doing so will cause the nonlinear threshold to be more difficult to reach. By using circular nanomembranes instead of our more conventional doubly-clamped NEMS beams this effect can be somewhat suppressed; it will then be possible at a given frequency to reach the nonlinear threshold at a lower driving power. We will use this to our advantage during future efforts, and investigate use of piezoelectric circular membrane based devices with diameters in the range from $\sim 1.5 - 2.5\ \mu m$.

The use of circular membranes will have another significant benefit: they also provide a much larger area for transduction. This makes for more efficient operation at higher frequencies and opens the possibility for use of fully piezoelectric transduction, which is impossible for small flexural NEMS devices in the high UHF / low microwave range. This could have important implications for our studies of anomalous phase noise, as we have already shown that the transduction method can significantly affect the magnitude of this noise (see Appendix A.3-(d)).

Our estimates, shown in Figure 4, are that a nanomembrane resonator driven at three times the critical amplitude, which employs phase noise suppression methods that we have developed in the DEFYS Program via nonlinear dynamics, should be capable of exceeding the Phase II DEFYS program metrics. We have already begun to explore fabrication and initial testing of nanomembrane devices towards these ends (Figure 5.)

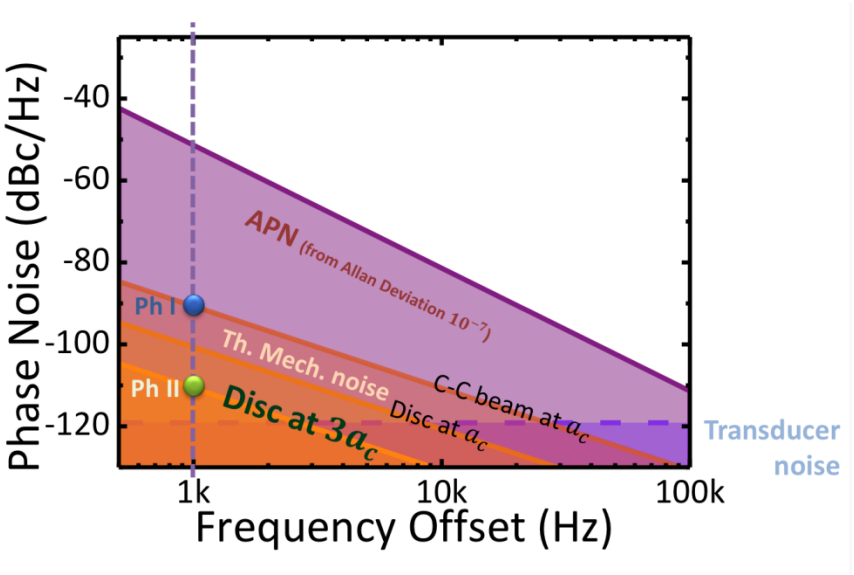

Figure 4: Estimated Phase Noise for 1 GHz Membrane Devices

The analysis takes into account APN (purple); and thermomechanical noise in: a clamped-clamped beam operating at the critical amplitude, a membrane operating at the critical amplitude, and a membrane operating at 3 times the critical amplitude. The latter is seen to meet the Phase II phase noise metric of -110 dBc at 1 kHz offset. The two dots correspond to the metrics for Phase I and Phase II, for the sake of comparison.

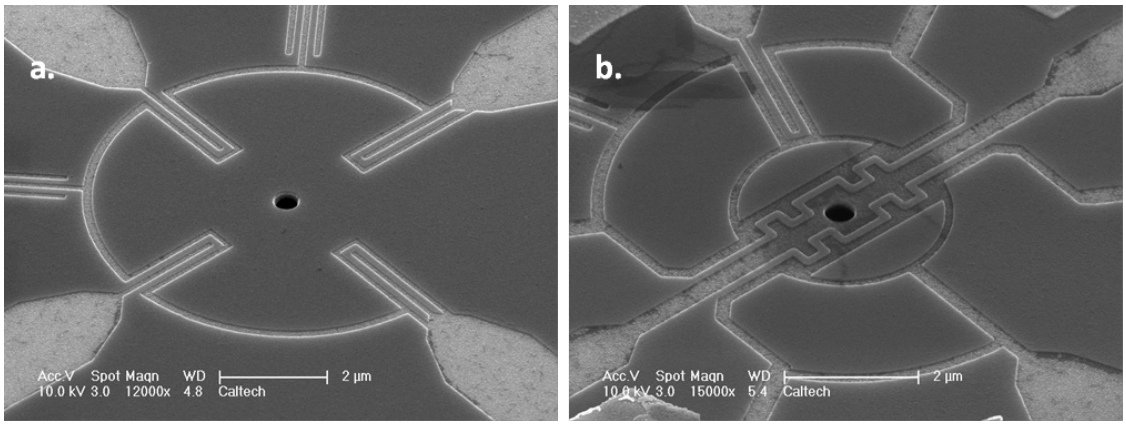

Figure 5: SEM Micrographs of Currently Fabricated Membrane Resonators with Piezoelectric Actuation and Piezometallic Detection

The temperature stability of the devices will be achieved using active temperature control, using a Ohmic heating element integrated on top of the membranes; a prototype is shown in Figure 5b. This approach is capable of allowing precise control with minute power consumption compared to that of macroscopic temperature control involving the entire silicon chip or package. To implement this step, and to integrate such devices into small-volume packaging, we will seek to maintain our successful and active collaboration with the team at Rockwell-Collins.

3.3 Development of Synchronized NEMS-Array Oscillators

Our theoretical estimations suggest that achieving improved metrics can be challenging with an individual oscillator, especially in the presence of anomalous phase noise. We therefore propose to employ multiple, synchronized NEMS oscillators to increase the total effective energy and decrease the phase noise for the coupled system. We propose to build arrays of nonlinear oscillators with electronically-engineered coupling and readout, as a complementary means for improving phase noise.

At the conclusion of this Program, we have successfully demonstrated synchronization of two coupled nonlinear oscillators and the suppression of the noise for this coupled system. This work is described in Appendix A.3-(e). This proof-of-concept demonstration has remarkable potential. It shows that NEMS oscillator synchronization is possible by straightforward engineering of external coupling and, thereby, that the expected enhancement factor of two, *i.e.* a 3dB reduction in phase noise, can readily be achieved.

Going forward, we believe it is therefore straightforward and natural to apply these concepts to NEMS through large-scale integration – and to expand the concept of a "device" to include systems that are, in fact, *arrays of nanodevices*, coherently coupled to provide net benefit surpassing that achievable from an individual element while being no larger than an individual microelectromechanical system (MEMS) device. For example, an array of approximately $N=10^2$ flexural NEMS oscillators would enable the Phase II DEFYS program metrics to be met, provided the APN is circumvented (Figure 3). If APN could not be completed suppressed, every 10 dB of APN about the metric could be circumvented by and extra order of magnitude of coupled resonators.

We believe that synchronization of a large number of disparate oscillators has application to a wide range of technologies beyond DEFYS, and the implementation in NEMS arrays will provide a paradigm for many other applications.

APPENDIX A - MAJOR EXPERIMENTAL ACCOMPLISHMENTS IN PHASE I

In our Phase I effort we have made a number of important advances in the engineering of NEMS device based nonlinear systems, have developed new methods for NEMS motion transduction, and have conceived of new oscillator architectures.

A.1 Bulk MEMS Devices

To demonstrate our ability to build oscillators at microwave frequencies and explore the phase noise performance limitations in more conventional, direct-drive oscillators, we have built microscale piezoelectrically-transduced Lamb-wave resonators. The resonators were originally fabricated within the context (and financial support) from another project to develop durable temperature sensors based on resonance frequency shift. A typical scanning electron microscope (SEM) micrograph of a device can be seen in Figure A1(a). The interdigitated electrodes on the left side are used to excite mechanical vibrations, and electrodes on the left side are used to detect the piezoelectric current generated by the elastic strain. To explore their use as oscillators we implemented a feedback loop using regular amplifiers with very low noise figure (NF), and performed phase noise measurements.

Results from one of our initial devices operating at f=2.2 GHz, with Q~300 and insertion loss ~14.5 dB are shown in Figure A1(b). For this device we measure a raw phase noise level of approximately -77 dBc/Hz @ 1 kHz offset (scaled to 1GHz). These tests were performed in a microwave probe station where insertion losses were not minimized. (As this is not our central DEFYS project, we did not take further steps to ameliorate these losses.) According to Everard[§], our level of insertion loss degrades the measured phase noise by approximately 5 dB, so we report an *intrinsic* phase noise level for this oscillator of -82 dBc/Hz @ 1 KHz offset.

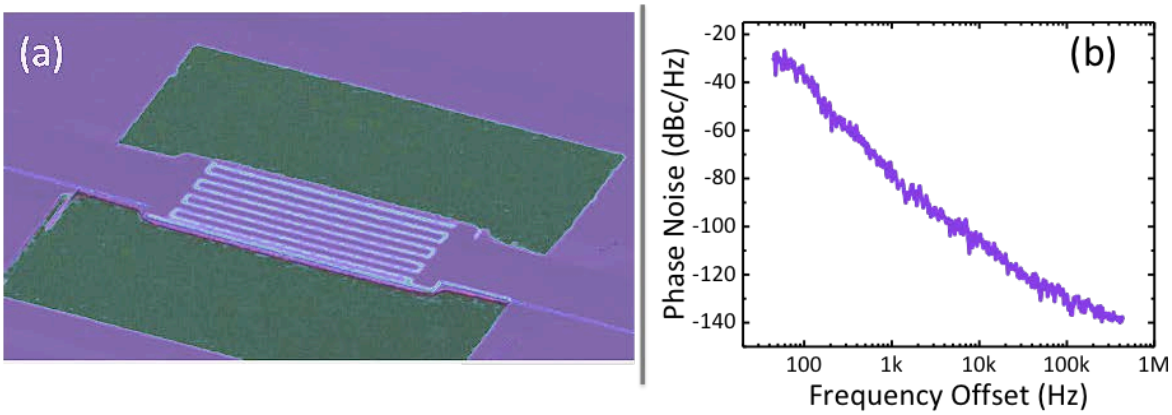

Figure A1: (a) An SEM Image of Microscale Bulk Piezoelectrically Transduced Linear Resonator (b) Uncorrected (Raw) Phase Noise Measurement

Measurement taken in the microwave probe station for a 2.2 GHz vibrational mode scaled to 1 GHz; correcting for the measurement insertion loss of 14.5dB (by 5dBc/Hz) yields an actual device phase noise of -82dBc/Hz at 1KHz.

[§] J. Everard, *"Low Phase Noise Oscillators: Theory and Application"*, 2009 Joint Meeting of the European Frequency and Time Forum and the IEEE International Frequency Control Symposium, Vols 1 and 2, Book Series: IEEE International Frequency Control Symposium, Pages: 338-343, DOI: 10.1109/FREQ.2009.5168197 (2009).

A.1.1 Recent Results: Bulk MEMS devices

Improved device fabrication has very recently yielded marked enhancement of device performance in our laboratory (Figure A2). Our recent Lamb-wave devices now provide Q's of order 1500 at f=1.5 GHz. Very recent probe station measurements for these devices provided a raw insertion loss (without any impedance matching circuitry) of approximately 20dB. Although at the time of the submission of this report we have not yet been able to carry out direct phase noise measurements on these devices, we can straightforwardly estimate their expected performance based on data we have obtained from the previous, similar, devices. With the Q improvement we have obtained over the previous devices (a factor of 5), and considering the additional 5dB insertion loss – these should yield factors of 14dB and 4dB[§] change, respectively, in the expected phase noise levels. These considerations lead us to expect that the phase noise performance of these improved devices (scaled to 1 GHz) should now be 18 dBc/Hz better, *i.e.* at the level of **-100dBc/Hz at 1kHz offset, which exceeds the DEFYS Phase I metric.**

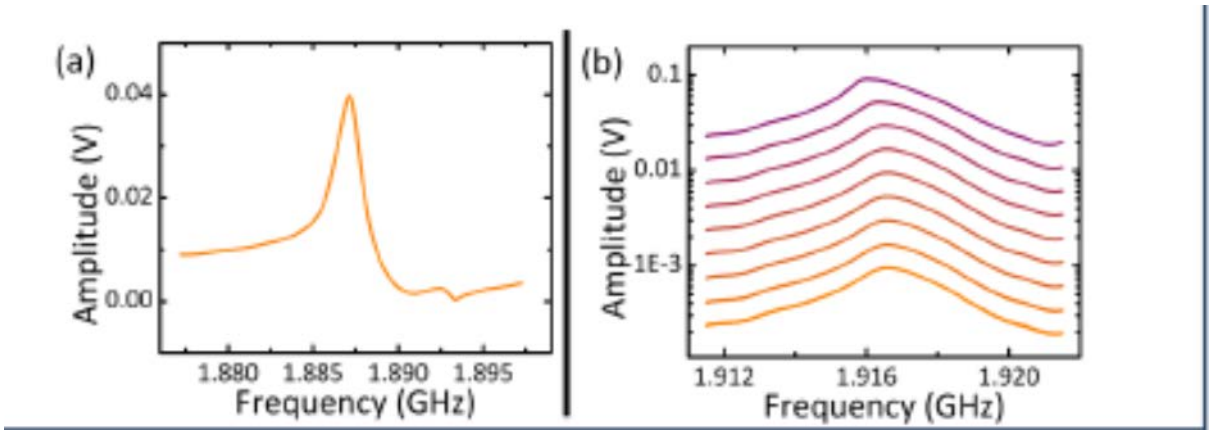

Figure A2: (a) Resonant response of a Second Generation Bulk-mode MEMS Device, showing Q = 1500 (b) Resonant response for different Driving Amplitudes (ranging from -30dBm to +10dBm) for a similar Device

It is very interesting to note that these devices show the onset of nonlinear behavior for very strong drive levels, *i.e.* beyond +10dBm. We find that the material stability of these devices is quite good at these high drive levels; our preliminary assessment is that they can be left apparently indefinitely without signs of fatigue under these high-level operating conditions.

A.2 Transduction Technology for NEMS Oscillators

In contrast to the bulk MEMS resonators shown above, piezoelectric transduction is very challenging to implement when the size of the resonator is reduced some orders of magnitude. Therefore, in order to efficiently transduce the mechanical signal into an electrical one, we developed a novel transduction technology with which most of the experiments within the first phase of the program have been conducted. This novel technique consists in a combination of piezoelectric actuation and piezoresistive detection, and it was developed specifically for this program. In addition to large transduction efficiency (within NEMS standards) this technique presents the advantages of large dynamic range (no transduction nonlinearity) and the possibility of

tune the frequency of the resonator, allowing not only for direct actuation but also for parametric actuation.
The resonators that we have typically used are flexural resonators with a structural multi-layer consisting of an ultrathin (50 nm) piezoelectric aluminum nitride (AlN) sandwiched between two molybdenum (Mo) layers deposited on top of AlN seed layer. We carefully analyzed the physics of the transduction scheme (see Figure A2(a)) and built an equivalent circuit model, shown in Figure A2(b).

The top electrode of the resonator was patterned in order to properly define an actuation part and a piezoresistive current loop for detection which dimensions and exact geometries depended on the main application or functionality sought for each device. The direct actuation efficiency is maximized when the actuation electrode (λ_{act} in Figure A3(a)) occupies approximately 1/3 of the beam length ($\lambda_{act} = L/3$). Alternatively, parametric actuation efficiency is maximized when most of the device is covered by the actuation electrode ($\lambda_{act} \approx L$ in Figure A2(a)). This trade-off between both actuation efficiencies is optimized at around $\lambda_{act} \approx 0.8L$, when the frequency tunability is optimized while keeping the direct drive efficiency at a high level.

When voltage is applied between the actuation electrode (shown in purple on the left side of the beam in Figure A3(a)) and the bottom metal layer (ground), a strain ε_1 proportional to the electric field E_3 develops in the active piezoelectric layer (shown in green). As the multi-layer is vertically asymmetric, such strain creates a bending moment, thus actuating mechanical motion. The amplitude of motion w, as a function of the frequency, ω, is:

$$w(\omega) \approx \chi(\lambda_{act}) \frac{d_{31} z_{offset\_PZE} L^2}{t_{total}^3} V_{in} \frac{1}{1 - \left(\frac{\omega}{\omega_0}\right)^2 + j\frac{\omega}{\omega_0 Q}} \quad (1)$$

where d_{31} is the piezoelectric constant of AlN, L and t_{total} are the length and thickness of the beam respectively, z_{offset_PZE} is the measure of the vertical offset of the piezoelectric layer from the elastic neutral axis, ω_0 and Q are the resonance frequency and quality factor of the resonator respectively, and $\chi(\lambda_{act})$ is a parameter that solely depends on the vibrational mode and on the actuation electrode length. The motion of the resonator causes a periodic strain modulation of the piezoresistive loop and, consequently, a modulation of the resistance value. Provided a direct current (DC) voltage bias V_{DC} is applied to the resistor, an alternating current (AC) current proportional to the amplitude of motion is generated. The motional current i_m as a function of the input voltage V_{in} and the physical parameters of the beam is:

$$i_m = \frac{V_{DC}}{R_{tot}} \frac{r_{loop}}{R_{tot}} \chi(\lambda_{act}) \xi(\lambda_{det}) \frac{G_{PZM} d_{31} z_{offset\_PZE} z_{offset\_PZM}}{t_{total}^3} V_{in} \frac{1}{1 - \left(\frac{\omega}{\omega_0}\right)^2 + j\frac{\omega}{\omega_0 Q}} \quad (2)$$

where z_{offset_PZM} is the vertical offset of the top metal layer from the elastic neutral axis, r_{loop} and R_{tot} are the loop resistance and total resistance including leads and pads respectively, G_{PZM} is the gauge factor of the metal in use (in our case Molybdenum), and $\xi(\lambda_{det})$ is a parameter that solely depends on the vibrational mode and on the loop geometry. Both constants ($\chi(\lambda_{act})$ and $\xi(\lambda_{det})$) are usually estimated via Finite Element Modeling (FEM) simulations prior to the fabrication, so that the geometry of both top electrodes is optimized.

The expression for motional current given by equation (2) is used to define the equivalent circuit for the described transduction technique (Figure A3(b)). The circuit includes the mechanical impedances, shown as L_m, C_m, and R_m in series, parasitic capacitances $C_{0\pm}$, feed-through capacitances $C_{ft\pm}$, the load impedance Z_L (in our case, it basically is R_{tot}), and a $\pi/2$ phase shifter, which is needed to account for the proper phase shift within the mechanical resonator. One of the major challenges with NEMS transduction is the direct feed-through of the actuation voltage to the detection port. This is caused by the actuation electrode exciting charges in the substrate that later are transferred to the detection port, and it is modeled as a feed-through capacitor C_{ft+}. In order to minimize this feed-through, it is possible to arrange the resonator in a bridge setup with a dummy electrode, patterned adjacent to the beam. By carefully balancing the signal sent to this second electrode, it is possible to compensate the feed-through from the actuation electrode, effect that is modeled via an additional capacitance, C_{ft-}. By doing so, it is possible to obtain a virtual ground at the detection port, thus canceling any undesirable radio frequency (RF) background, given the fact that mechanical signals substantially larger than direct RF feed-through are especially important to implement self-sustained oscillators.

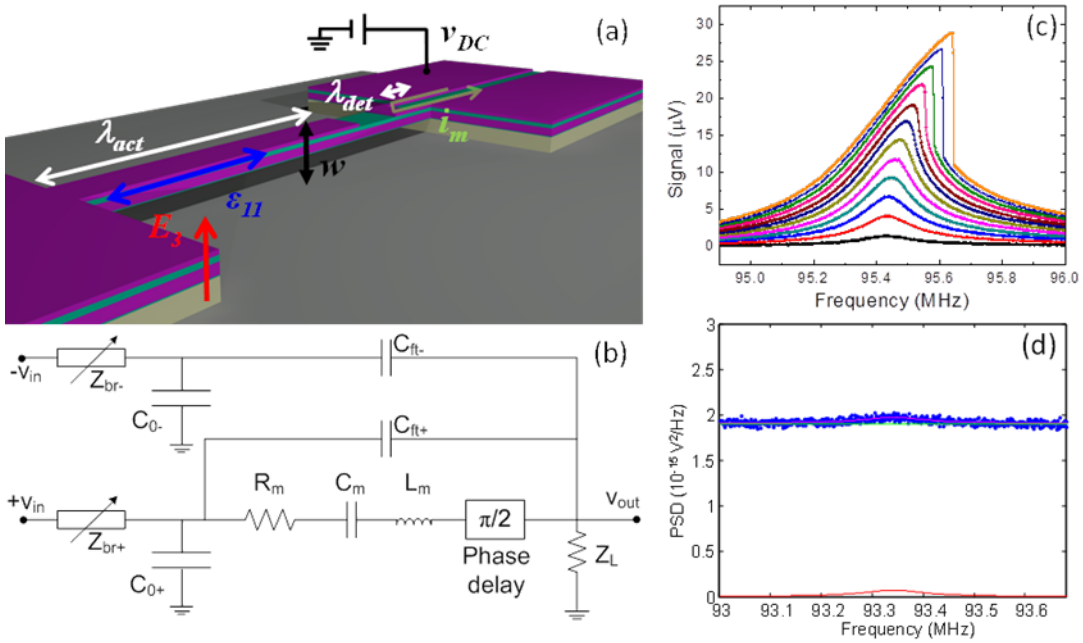

Figure A3: (a) Diagram showing the Physics of Piezoelectric-Piezoresistive (PZE-PZR) Transduction Method (b) Equivalent Circuit of PZE-PZR (c) Spectral response of a typical Resonator in Open Loop at different Drive Levels (d) Thermomechanical Noise Measurements
Notes for figures: (a) The piezoelectric layer (green) is sandwiched between two metallic layers (purple); (b) It includes two balancing bridge impedances, parasitic capacitance, load impedance, and equivalent mechanical LCR circuit; (d) , Data is shown in scattered blue plot, system noise is shown in green, Lorentz fit in purple and pure resonator Brownian motion is shown in red.

The described transduction has been used to characterize the mechanical motion of doubly clamped beams, with fundamental resonance frequencies from 5 MHz up to 250 MHz. In particular, Figure A3(c) shows the response of a 95 MHz beam, with dimensions $L \cdot W \cdot t = 4\mu\text{m} \cdot 450\text{nm} \cdot 210\text{nm}$. The network analyzer scans of the resonance response, taken at different drive levels, are shown in Figure A3(c). The piezometallic detection is in this case sensitive enough so that the

thermomechanical motion of the resonator is visible. The power spectral density of the noise of the system is shown in Figure A3(d). The measured data are shown as the blue scatter plot and its Lorentzian fit is shown in purple. The total output signal consisted of the thermomechanical noise of the Brownian motion of the resonator's fundamental mode (red) and system noise, shown in green, composed almost equally by the Johnson noise of the resistor and the input noise of the amplifier.

A.2.1 Characterization of Nonlinearity

As mentioned above, one of the major advantages of the developed transduction technique is that it presents a remarkable dynamic range, therefore enabling careful characterization of the nonlinear properties. The complete quantitative characterization and understanding of NEMS resonators nonlinear properties is crucial for the development of dynamics enabled oscillators.

In order to perform a systematic study of the nonlinear mechanics at the nanoscale, the transduction of the mechanical motion into electronic signals must be accurately calibrated. This calibration is performed using an inherently nanoscale phenomenon, the random Brownian motion of the mechanical resonator. As the transduction technique is very sensitive, it is possible to detect such motion electrically and therefore calculate the conversion to mechanical deflection, using the equipartition theorem.

In particular, a careful study was performed using a device operating at 14.3MHz, with dimensions: $L \cdot W \cdot t = 9\mu\text{m} \cdot 450\text{nm} \cdot 210\text{nm}$. The schematic of the measurement setup together with a SEM image are shown in Figure A4(a). The comparison between experimental Duffing nonlinear resonance measurement and Euler-Bernoulli theory is shown in Figure A4(b). The network analyzer frequency up sweep is shown in black and the down sweep is shown in blue. Hysteretic behavior is evident and its theoretical prediction including the unstable solution is shown in red.

We characterized the Duffing nonlinear coefficient of the first three flexural out-of-plane vibration modes of the beam. The squared amplitude of the second mode taken at different drive levels is shown in the top graph of Figure A4(c). The linear fit of the dependence of the curve maximums on frequency was used to extract the nonlinear Duffing coefficients of the vibrational harmonics.

Our remarkable transduction technique also allowed us to characterize the nonlinear interaction between the modes. The complete quantitative knowledge of these coefficients was important to determine the fundamental limitation on oscillator phase noise due to the influence from other vibrational modes. The coupling manifested itself in the shift of the frequency of a particular vibrational mode due to the high amplitude motion of the other modes. Since the Duffing nonlinearity caused frequency detuning at high excitation levels we could characterize the coupling by measuring the detuning of one mode driven at low level (mode *k*) as a function of frequency detuning of the mode driven at high level (mode *j*), by introducing dimensionless coefficient $\nu_{jk}: \frac{\Delta\omega_k}{\omega_\text{k}} = \nu_{jk}\frac{\Delta\omega_j}{\omega_j}$. Examples of the plots for low level mode 3 and high level mode 2 are shown in the bottom panel of Figure A4(c).

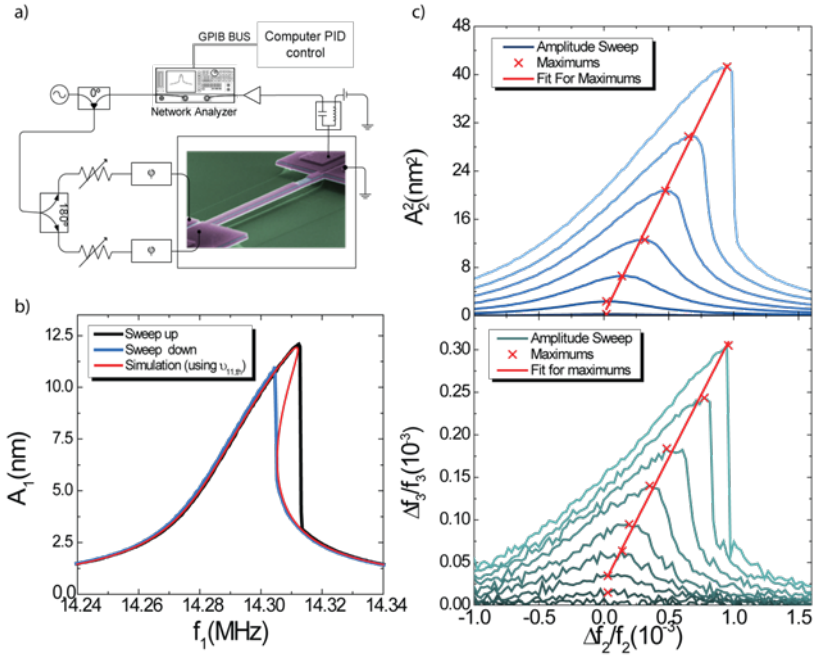

Figure A4: (a) Schematics of the setup for Measuring Nonlinear Coupling Coefficients (b) Calculation of Frequency sweep using the Theoretical Value for the Duffing Nonlinearity (red) with the Experimental Data shown for up sweep (black) and down sweep (blue) (c) Measurements of the Coupling Coefficients. The top graph gives the diagonal components of the matrix. The relation between the two vertical scales gives the off-diagonal components.

After calibrating the displacement with the thermomechanical noise, we ascertain these coefficients by performing two sets of experiments: first we determined the diagonal terms ν_{kk} by sweeping the amplitude and frequency of a single mode *k* (*k*=1,2,3) (Figure A4-top). Then we swept the frequency of mode *j* different from *k* and monitored the resonant frequency of mode *j* to determine the coupling strength ν_{jk} (Figure A4(c)-bottom). The relationship between the two vertical scales shown gives ν_{jk}. We use a digital PLL circuit with a network analyzer as shown in Figure A4(a) to monitor the mode *j* frequency. The results are shown in Table A-1, with theoretical predictions given in parentheses.

We find excellent agreement between the theoretical calculations and experimental measurements for the diagonal terms ν_{kk}, the Duffing coefficients as indicated in Figure A3(b). The cross-coupling terms yield good agreement as well, most of them within 6% of the expected values. The terms ν_{12} and ν_{23} are about 20% out of the expected values, indicating a larger deviation from Euler-Bernoulli theory.

Table A-1. Nonlinear Coupling Coefficients

ν_{jk} $(\cdot 10^5)$	Driven 1	Driven 2	Driven 3
Sensed 1	0.55±0.10 (.546)	1.76±0.36 (1.49)	3.51±0.47 (3.70)
Sensed 2	0.18±0.01 (0.189)	1.19±0.03 (1.17)	1.77±0.13 (1.67)
Sensed 3	0.13±0.01 (0.125)	0.35±0.06 (0.449)	1.49±.07 (1.44)

A.2.2 Flexural Modes in NEMS Membranes

Most of the experimental work performed during Phase I of this project has been done using clamped-clamped beams. However, experimental evidence seems to point out the need of being able to store more energy in the system, having better transduction gain. The best structure that can allow us to do so, simultaneously keeping the nonlinear threshold at a reachable level, are nanoelectromechanical membranes operating in flexural modes. As an illustrative example of what can be achieved, Figure A5 shows the drive amplitude sweep frequency response of two degenerated vibrational modes in a 4μm in diameter membrane.

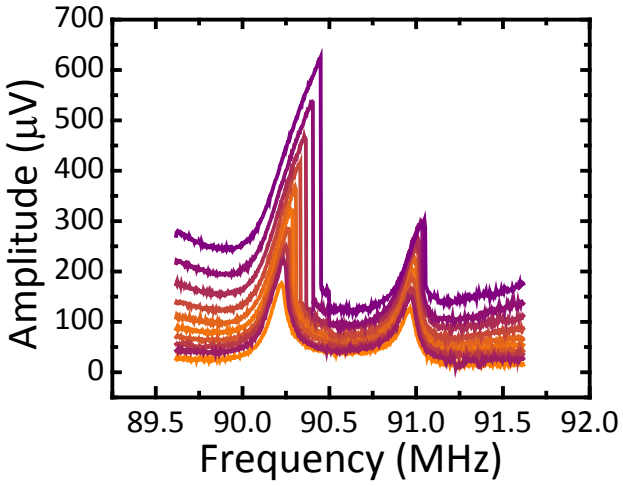

Figure A5: Amplitude sweep Frequency response of two Modes in a 4μm in Diameter Membrane

A.3 Directly Driven NEMS Oscillators

A.3.1 High Frequency Oscillator

We have routinely built and studied nanomechanical oscillators transduced by the above-described technique. To illustrate the efficiency of our NEMS transduction technique we were able to demonstrate the highest frequency nanomechanical oscillator operating at room temperature to date. Figure A6(a) shows the S_{21} transmission characteristics achieved for a 3 μm long, 180 MHz doubly clamped beam, after achieving sufficient RF background compensation with the bridging technique and employing narrow bandpass filter. With such device, we built a self-sustained oscillator. A typical phase noise measurement is shown in Figure A6(b).

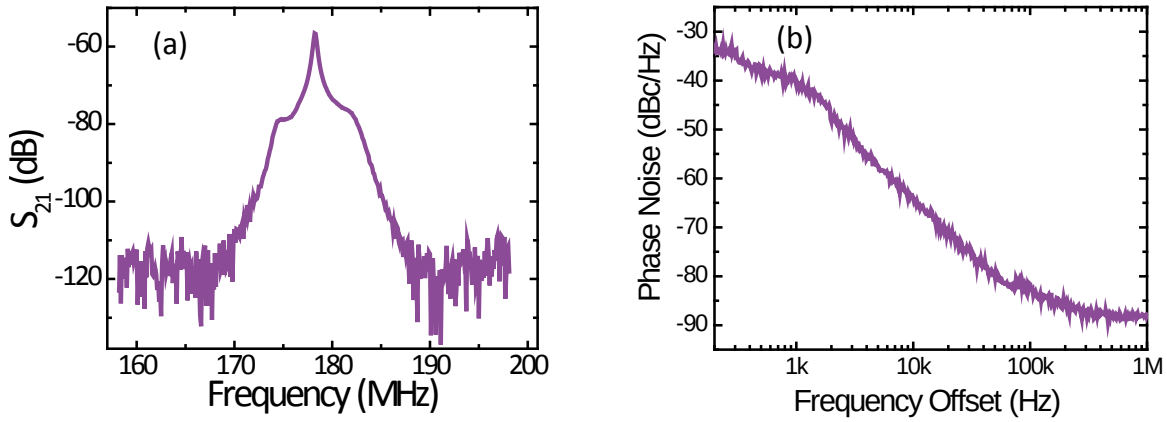

Figure A6: (a) Transmission Characteristic obtained for 180 MHz Nanomechanical Doubly-clamped Beam (b) Phase Noise Measurement of the highest Frequency NEMS Oscillator operating at Room Temperature

A.3.2 Backbone Control

As it is shown in Appendix B, we have made substantial progress in understanding the dynamics of an oscillator based on a nonlinear resonator as a complete nonlinear system. In particular, we have theoretically analyzed various noise sources and developed techniques to implement nonlinear dynamics enabled noise reduction strategies. The first example consists in the control of the nonlinearity in NEMS resonators by tweaking a control parameter involved in the transduction technique already presented, the resistor bias voltage V_{DC}. When such bias voltage is increased, Joule heating of the resistor modifies the stress distribution of the doubly clamped beam. This, together with the selective removal of parts of top electrode, since the different layers in our film had different built-in stresses, allowed for a control of the initial deformation of the resonator.

The structural multi-layer in the performed experiment consisted of 50 nm piezoelectric AlN sandwiched between a 40 nm Mo layer on top and a 100 nm layer below, grown on top of a 20 nm AlN seed layer. The layers are sputtered by a dc pulsed magnetron reactive process where the built-in stress is controlled to minimize the total stress for the whole structure, thus creating unequal stresses in composite layers. Therefore, the beam deflects when the top electrode is partially removed. By changing the lengths λ_{act} and λ_{det}, the initial deflection is modified.

In addition, the variation of V_{DC} yields the capability of a finer control of the deflection by changing the current passing through the piezoresistor and therefore it modulates Joule heating. The thermal gradient alters the initial deflection. This initial deflection is equivalent to a large offset force that affects the effective nonlinear coefficient. Thus, modifications in the initial deflection translate directly into modifications of the nonlinear coefficient.

The increase in V_{DC} makes the nonlinear behavior of the beam more soften. In a certain range of currents, the backbone curve exhibits mixed behavior – the frequency is first pulled in one direction and subsequently in the opposite direction as the drive amplitude is increased. In this range the backbone curve possesses an extremum we call the "sweet spot". If a self-sustained oscillator was biased close to the "sweet spot", the phase noise originating from amplitude-frequency conversion is reduced.

We performed careful studies of the backbone control capabilities using our lower frequency resonators. A SEM micrograph of a device with dimensions $L \cdot W \cdot t = 8\mu m \cdot 550nm \cdot 210nm$ is shown in Figure A7(a). The family of measured backbone curves (scattered black) and their fourth degree polynomial fits (red), measured at different biases, are shown in Figure A7(b). This result indicates that the amplitude of oscillation at the "sweet spot" could be tuned within a certain range. Figure A7(c) shows the amplitude of the "sweet spot" as a function of the DC bias. We demonstrated an effective increase in power of 10 dB with consequent reduction in phase noise could be possible with this method.

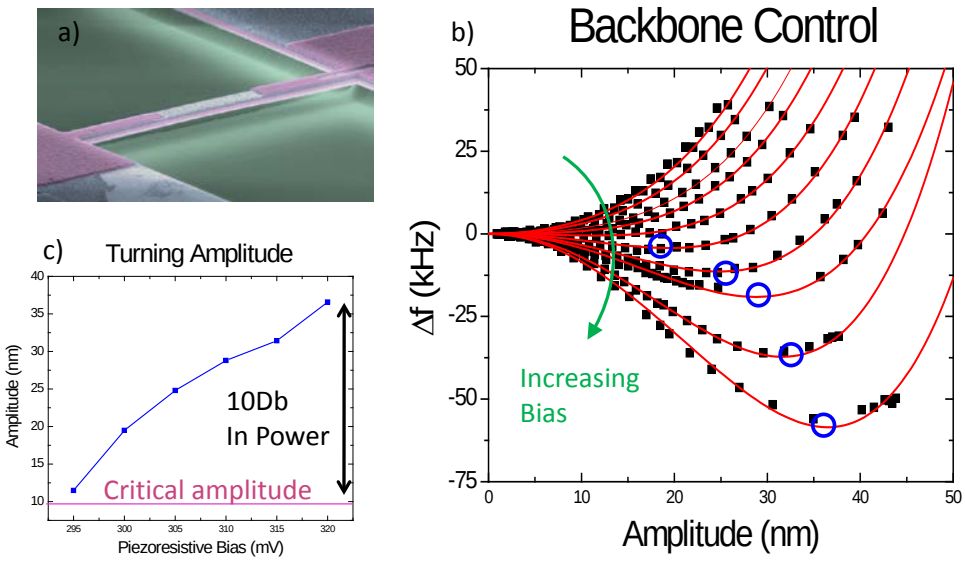

Figure A7. (a) SEM image of NEMS Resonator designed for Backbone Control Experiment (b) Measured Nonlinear Frequency pulling Curves taken at increasing DC Biases. Fourth Degree Polynomial Fits are shown in red (c) Amplitude of the "Sweet Spot" as a function of applied DC Bias: a 10dB enhancement in power is possible with this Method

After we mapped the input parameter space with the driven resonator, thus determining the bias and phase parameters necessary to operate the oscillator at an extremum point, we built an oscillator and characterized its performance under varying conditions including the piezoresistive bias and feedback phase. We set the bias and slowly swept the feedback phase parameter while monitoring the frequency of self-oscillations. Figure A8(a) shows the corresponding measurement results. We

were able to observe phase noise reduction at the extremum point of the frequency-amplitude plot. The two phase noise plots in Figure A8(b) were taken at the beginning of the feedback phase sweep (orange) and at the extremum (purple).

After careful examination of the limitations we concluded that the frequency scalability of this method for nonlinearity control was restricted. We believe the unification of the backbone control thrust with our parametric feedback oscillator effort was more beneficial, as the parametric feedback might provide an alternative mechanism for backbone control. Then the combination of two feedback loops, where direct drive feedback loop sustains the oscillations and parametric loop modified nonlinear properties, had a potential of significant oscillator performance improvement.

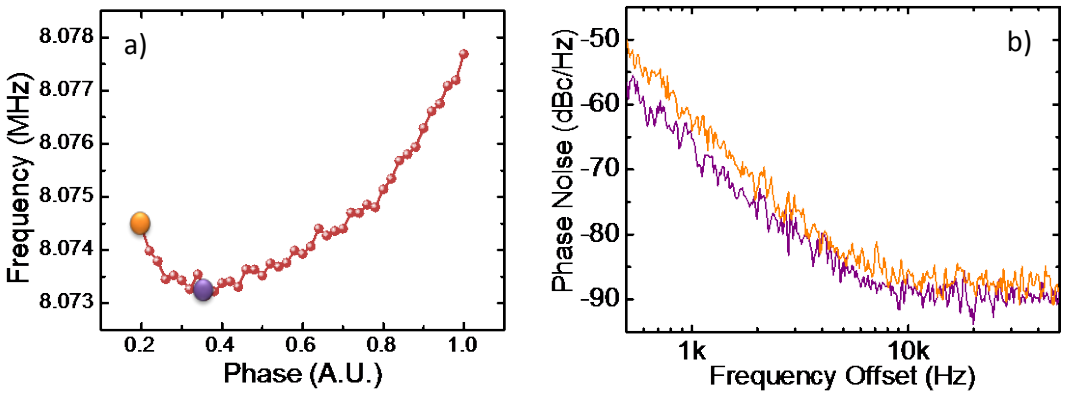

Figure A8: (a) Dependence of the Oscillation Frequency on the Feedback Phase (b) Phase Noise Reduction

The orange plot shows the phase noise measurement at the beginning of the sweep shown in (a); the purple plot shows measurements at the extremum point. The corresponding data points are indicated in (a) as the orange and purple marker respectively. As the dominant source of noise in this experiment was unknown, it is unclear whether the noise optimization was obtained due to be working in the "sweet spot" or by reduction of the contribution due to fluctuations in the phase Δ.

A.3.3 Yurke & Kenig Points

As it is shown in Appendix B, we have made substantial progress in understanding the dynamics of an oscillator based on a nonlinear resonator as a complete nonlinear system. In particular, we have carefully analyzed all the sources of noise that contribute to a direct drive oscillator phase noise, focusing in the case of heavily saturated oscillator.

As explained in Appendix B, when an oscillator is heavily saturated, the phase diffusion (phase noise) is going to be affected by noise in the following parameters: the resonant frequency ω_0, the nonlinear parameter α, the linear dissipation Q, the saturation S, and the feedback loop phase Δ. In addition, thermomechanical noise also affects the phase noise by directly feeding in the phase quadrature and, due to the resonator nonlinearity, via amplitude-phase conversion.

Our analysis has some points in common to that performed by Yurke *et al.* in 1990, but we have expanded it to include additional sources of noise. As illustrated in Figure B1(a), we have found that there are two types of points where the resonator nonlinearity can be used to cancel the contribution to the phase noise of certain parameters. The first type of points corresponds to those for which $d\Omega/d\Delta = 0$, and they will be called Yurke points to acknowledge that he used this concept back in

1990. We, however, have noticed that there are two values of Δ per each saturation S (above the onset of nonlinearity) that make $d\Omega/d\Delta = 0$. These two points are marked with red circles in Figure B1(a). The second type of points corresponds to those for which $\partial\Omega/\partial a = 0$, or Kenig points. Whenever the oscillator operates at those points, the amplitude and the phase are detached, and no amplitude-phase conversion can occur. This is a major development because that is the major deterrent to operate mechanical resonators beyond their critical amplitude, the amplitude-phase conversion due to their nonlinearity (these points are marked in Figure B1(a) as green stars). As it can be seen in Figure B1(a), one of the Yurke points is very close to Kenig point, meaning that there is a region where both amplitude-phase conversion and noise in the phase Δ can be minimized.

In order to experimentally prove the theoretical predictions, we utilized a clamped-clamped beam operating at low frequency (13 MHz) with dimensions: $L \cdot W \cdot t = 8\mu m \cdot 450nm \cdot 175nm$, with the transduction technique already introduced above (piezoelectric-piezometallic). A feedback loop with several amplifiers, phase shifters and limiters was set-up in order to obtain the final heavily saturated oscillator, as it can be seen in Figure A9(a). In order to prove that the oscillator was operating in the heavily saturated regime, it is possible to plot oscillation amplitude versus the oscillation frequency (for different values of Δ and S) and compare those results with the open loop response of the nonlinear resonator, as it can be seen in Figure A9(b).

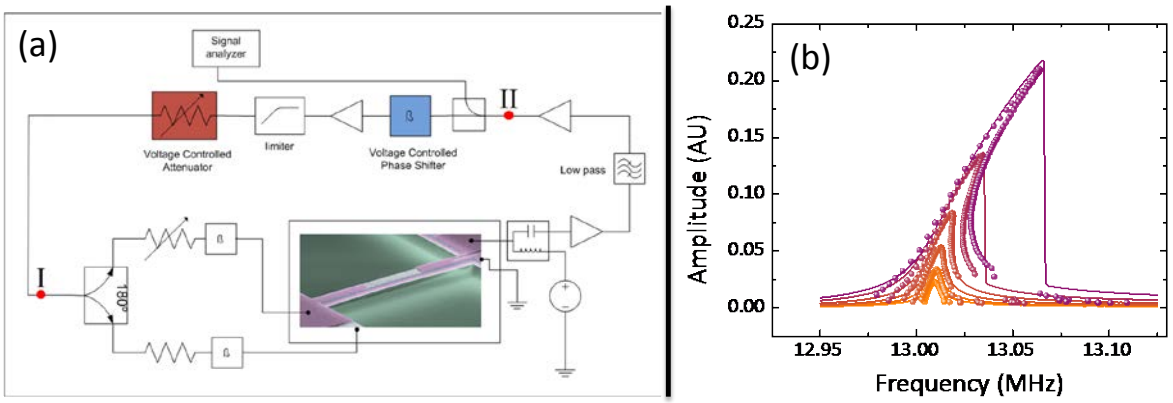

Figure A9: (a) Schematic of the Circuit used to perform this Experiment, including a SEM Micrograph of the low Frequency Device utilized (b) Superimposed Open Loop response of the driven Nonlinear Resonator (solid lines) with Amplitude-frequency operating points for the Closed-loop system for different values of Δ and S

The agreement of both sets of data evidences we operate in the heavily saturated regime.

In addition to monitoring the amplitude and frequency of the oscillator while changing S and Δ, we also measured the phase noise for each particular operating point. We can show the results by plotting the phase noise at 1 kHz offset as a function of the phase Δ for different S, as it is shown in Figure A10. The confirmation of the theoretical predictions is a major development in the understanding of phase noise in nonlinear oscillators. Even though we have only shown this for a low frequency oscillator, the result should be applicable to any oscillator that shows nonlinear behavior.

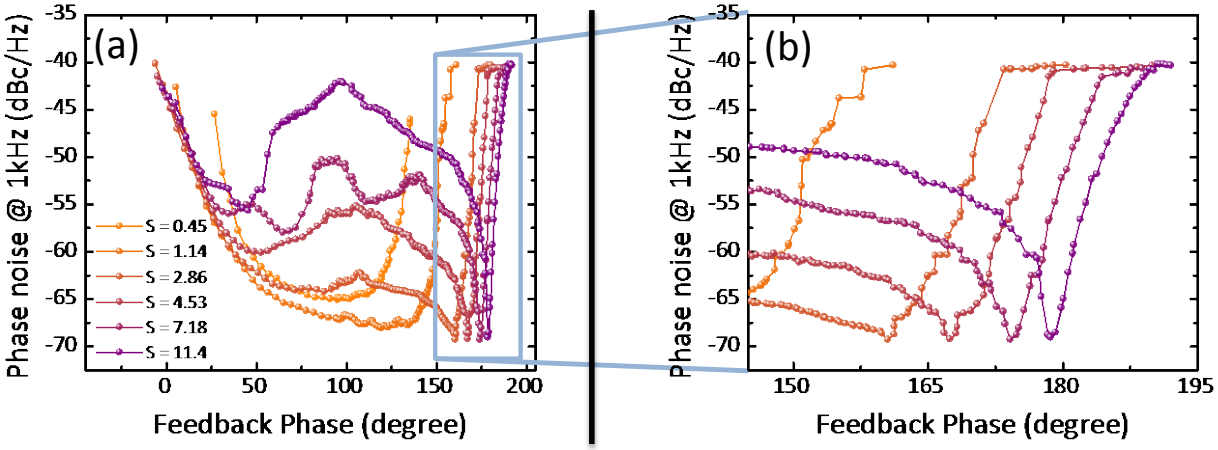

Figure A10: (a) Phase Noise in the low Frequency heavily-saturated Oscillator at 1kHz offset as a function of the Feedback Phase (Δ) and for different values of the Saturation Drive (*S*). As predicted, a sharp drop in the Phase Noise is observed in the proximity of the Kenig-Yurke's pair of points (b) Zoom in the Region with the sharp decrease

A.3.4 Anomalous Phase Noise

By using the previously presented techniques for phase noise reduction, we were able to show an improvement in the performance, but still the experimentally obtained phase noise was significantly higher than the ultimate performance limitation, set by thermomechanical noise, and originally estimated in the proposal. We attributed these observations to the presence of a previously unknown noise source, related to direct fluctuations in the resonator's eigenfrequency.

We performed several studies of the limitation of frequency stability in our nanoscale nonlinear resonators and found characteristic behavior consistent with direct noise in the resonance frequency of the mechanical structure. We refer to this process as APN, since we do not understand its origins. Unfortunately, this noise directly feeds into the phase noise of the oscillator, and therefore it is impossible to eliminate by means of modifications in the oscillator dynamics, without understanding the underlying physical mechanism.

A brief survey of the literature and the knowledge base from previous projects in our lab indicated that APN was relevant in all observed nanoscale mechanical structures. Several important observations could be made about this noise:

- The AD does not decrease with the drive above a certain drive level
- That saturation of the AD occurs for the whole range of integration times tested (100ms-10s)
- Off-resonance noise is consistent with the resistor Johnson noise
- The on-resonance noise power spectral density rises linearly proportionally to the signal
- The noise power is asymmetric with respect to quadrature
- The phase quadrature and power of the noise as a function of drive is consistent with frequency noise

We performed several studies with the purpose of determining the nature and properties of this noise. Most of the previous observations of frequency stability of nanoscale mechanical structures in the research community were performed in the context of driven resonator frequency measurements, typically characterized by Allan deviation. Oscillator phase noise and resonator Allan deviation measurement are equivalent in characterizing the NEMS frequency stability. The main difference involves typical uses of the two methods: Allan deviation is usually employed to ascertain frequency stability on longer time scales – above 100 ms, while the phase noise metric is normally used for shorter time scales – below 10ms (above 100 Hz offset). In order to achieve a fair comparison, we therefore performed Allan deviation measurements of our NEMS devices when used as driven resonators. We performed measurements with both closed loop, when the drive frequency was continuously adjusted, and open loop, when drive frequency was kept constant and the changes in phase of the signal were measured. The phase change signal was later translated to a change in frequency and plotted as Allan deviation. Open and closed loop methods were proved to be equivalent both theoretically and experimentally.

As a particular example of the experiments performed, we present here the use of a nanomechanical resonator with piezoelectric actuation and piezometallic detection, the transduction method previously described. The device was driven continuously on resonance and its frequency was monitored over the course of several hours. As we increased the resonator's amplitude of motion, if the thermomechanical noise were the limiting factor, then the corresponding AD would continuously decrease. We observed a different behavior. In Figure A11 the AD at 1s averaging time is plotted as a function of drive power. The three different plots correspond to three piezoresistive DC biases: 50 mV – blue, 100 mV – red, 200 mV – green.

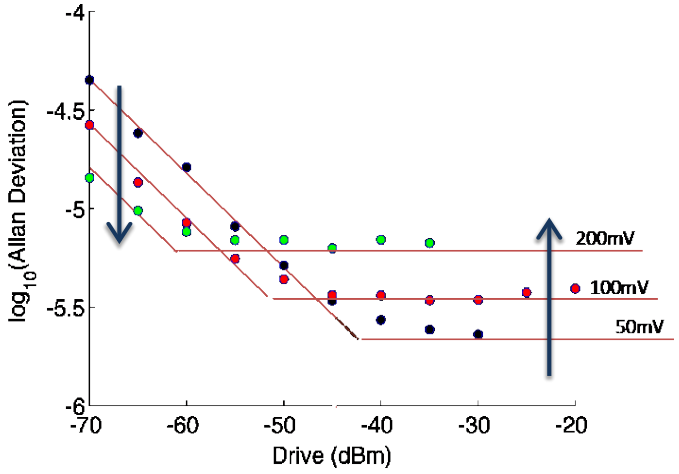

Figure A11: Allan deviation at 1 second averaging Time is plotted as a function of Resonator's Drive Power

Three different color markers represent three different piezoresistive biases.

At small drives the thermal white noise is dominant; therefore increasing drive leads to decreasing Allan deviation. Also the increase in piezoresistive bias caused improved detection efficiency and thus larger output signal, which in turn led to a decrease in the AD. This is due to the fact that, as previously mentioned, our noise in the system is limited by Johnson noise in the resistor and amplifier input noise, which do not change with the bias, while the signal does. However, at larger drives the Allan deviation saturated and stayed constant while the drive power was substantially enhanced. This behavior is expected if fluctuations in the resonance frequency are the dominant

noise source. Importantly, the saturation level seems to be lower at lower biases, which might be an indication of the dependence of APN upon the piezoresistive bias. More experiments need to be performed before anything conclusive can be stated.

A.3.5 Synchronization of Coupled Oscillators

As already introduced in the proposal, we strongly believe that the great comparative advantage of NEMS-based oscillators is the possibility of using synchronization to reduce the phase noise of the total system. Therefore, we implemented a system with two coupled low-frequency nonlinear oscillators. To do so, we utilized two clamped-clamped beams with dimensions: $L \cdot W \cdot t = 8\mu m \cdot 450nm \cdot 175nm$, operating at 13 MHz, and using the transduction technique already introduced above (piezoelectric-piezometallic). The coupling was implemented using a third feedback loop to combine signals proportional to the amplitude of each oscillator and sending them back as a driving force Figure A12. This scheme allowed unprecedented control of the parameters of the two oscillators, and the parameters could be quantitatively measured independently of the synchronization experiments.

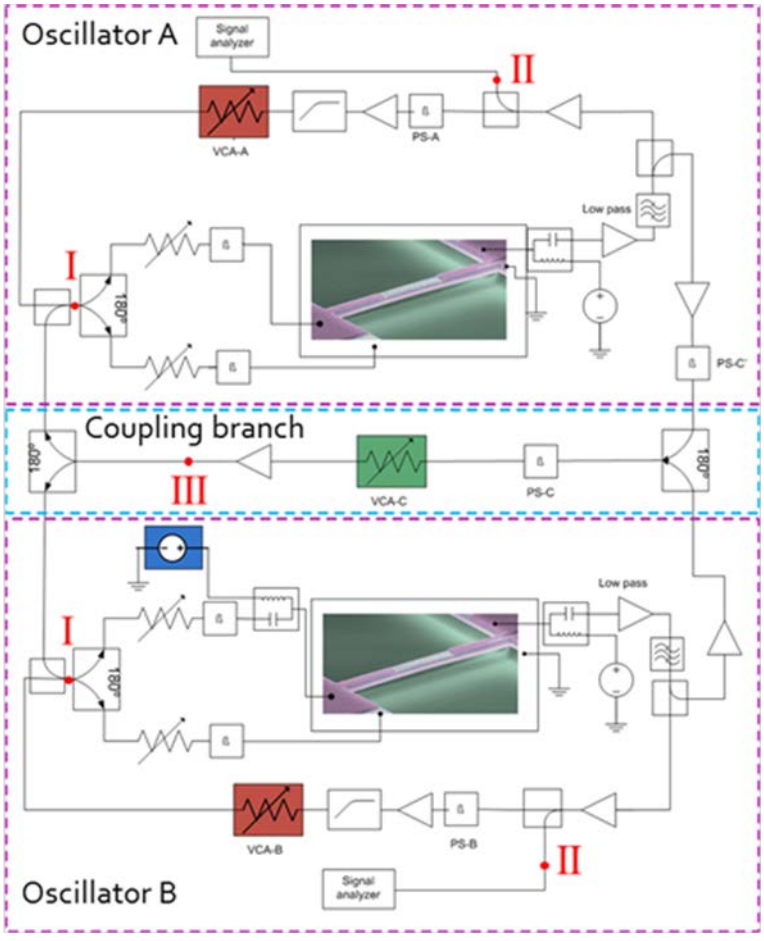

Figure A12: Experimental setup for Oscillator Synchronization using a Feedback Loop (blue dashed box) to form an effective Coupling

We can tune detuning using the voltage control on oscillator B (blue box), shear by tuning saturation (red boxes), and coupling by attenuating the feedback loop (green box).

The dynamics of the system was thoroughly explored within the broad parameter space relevant for operation. As an example, we will show here results for the low coupling limit, where we approximate the dynamics of the coupled oscillators using the Adler equation. In that case, the phase coupling parameter only depends on the nonlinear coefficient and the coupling coefficient of the oscillators:

$$\frac{d\phi}{dT} = \Delta\omega - 4\alpha_{kk}\beta_{kk}\sin\phi \tag{3}$$

where ϕ is the difference in phase between the two oscillators, $d\phi/dT$ is therefore the oscillators frequencies difference, $\Delta\omega$ is the difference of the original (open-loop) resonator frequencies, α_{kk} is the strength of amplitude-frequency coupling (a measure of the nonlinear coefficient), and β_{kk} is the coupling between both oscillators. In Figure A12(a) we show the experimentally measured oscillating frequencies difference as a function of the original detuning ($\Delta\omega$). Synchronization is observed when the phase of both oscillators advance at the same rate, i.e. $d\phi/dT = 0$. A range of intrinsic frequency difference leading to synchronization that grew with increasing coupling was clearly observed. As shown in Figure A13(a), the experimentally obtained data (black scattered data) are well described by the Adler equation (note that no fitting was performed in this case, the parameters were independently calculated by characterizing the feedback loops).

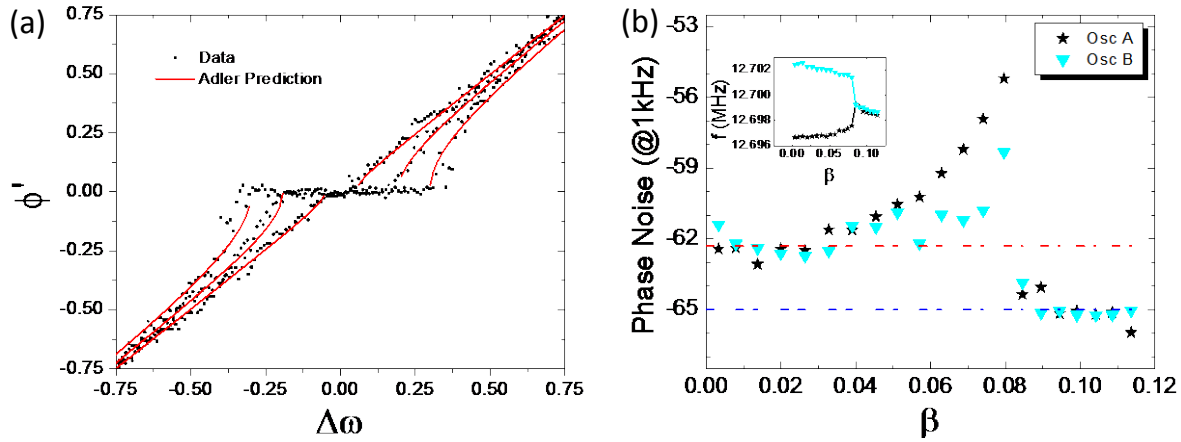

Figure A13: (a) Experimentally obtained (black scattered) Data for the Oscillators Frequency difference as a function of the original detuning ($\Delta\omega$). The system is accurately described by the Adler equation, with no fitting parameters. (b) Phase Noise of both Oscillators at 1kHz offset as a function of the coupling coefficient

The unsynchronized state shows higher phase noise than the synchronized state. In particular, a drop of 3dB can be observed when comparing the uncoupled system to the system just above the frequency locking threshold. This is attributed to the synchronization of the oscillators. Inset: frequency of both oscillators as a function of the coupling coefficient. The frequencies lock at the same point as the phase noise drops.

In order to prove the potential of synchronization for phase noise reduction, we then examined the phase noise for the two oscillators. In Figure A13(b) we show the phase noise at 1kHz offset as a function of the coupling coefficient between both oscillators, β. We observe that the phase noise starts at a value of -62dBc/Hz. As the coupling is increased, the apparent noise rises due to amplitude modulation of the two oscillators as they beat against each other when unsynchronized.

At a certain critical value of coupling the frequencies lock (see inset) and the noise drops to -65dBc/Hz. This 3dB drop is the result predicted for the synchronization of two separate oscillators.

A.4 Parametric Feedback Oscillator

A.4.1 Original Demonstration

In all the experimental work described up to here, the oscillator feedback has been exclusively limited to linear gain feedback proportional to the resonator output or, in the case of heavily saturated oscillators, with a saturation of the feedback signal due to amplifier nonlinearity and/or limiters. During the Phase I of this program, we have generalized the concept of an oscillator by implementing a feedback loop with a different transfer function. We experimentally demonstrated stable self-sustained oscillations using a cubic polynomial feedback transfer function, and we identified several potential advantages of such a generalized feedback technique. We showed that the generalized feedback loop is capable of accessing higher amplitude of operation, it eliminates the undesirable crosstalk, and it provides high level control of system parameters such as oscillation frequency and nonlinear coefficients. We analyzed the feedback loop and resonator as a combined nonlinear dynamical system, and we experimentally demonstrated improved phase noise performance and wide range frequency tuning.

We achieved the cubic feedback transfer function by applying a signal proportional to the square of the mechanical motion to the parametrically modulated the spring constant of the doubly clamped beam. In the first quarter of the DEFYS effort we fabricated NEMS doubly clamped beams optimized for efficient parametric frequency tuning, by covering most of the beam with a top electrode (as previously described). We demonstrated efficient parametric actuation with relatively low threshold values. During the second quarter we successfully implemented cubic feedback for the described devices operating at 15 MHz resonance frequency with dimensions:$L \cdot W \cdot t = 9\mu\text{m} \cdot 450\text{nm} \cdot 210\text{nm}$.

The schematic of the nonlinear feedback is shown in Figure A13(a). The mechanical motion close to the resonance frequency ω is electrically transduced by means of the piezometallic gauge effect. The signal is then amplified and filtered to suppress higher order harmonics. The signal is subsequently passed through a voltage controlled phase shifter and a nonlinear element which is optimized to generate a second harmonic at 2ω with amplitude proportional to the square of the input. In this proof of principle demonstration we accomplished the nonlinear transfer function by cascading two off chip amplifiers, so that they operated in saturation. We characterized the transfer function and found that it closely followed quadratic gain with a saturation term: $|V_{out}| = \Gamma|V_{in}|^2/(1 + (\Gamma|V_{in}|^2)/S)$, where Γ is the gain and S is the saturation level. The squared signal is then bandpass filtered around 2ω and applied to the parametric input of the mechanical device, which was the top electrode in our case. Since the feedback signal needs to be higher than the parametric threshold to excite the mechanical motion, the oscillator needs to be kick started by an external source. After the inception of oscillation, however, the starting drive can be turned off.

We analyzed the dynamical system of the periodically forced oscillators (PFO) using the secular perturbation method and obtained the following equation of motion of scaled amplitude *A* of an envelope of the signal:

$$\frac{dA}{dT}+\frac{1}{2}A-\frac{3\mathrm{i}-\eta}{8}|A|^2A=-\frac{1}{16}\frac{\Gamma|A|^2}{1+\frac{\Gamma}{S}|A|^2}A\mathrm{e}^{\mathrm{i}\Delta} \tag{4}$$

Equation (4) implies that the external parameters: gain Γ, and phase Δ, are able to control the effective nonlinear Duffing coefficient (equal to $3i/8$ in the original equation) or viscous damping (originally $\eta/8$). We experimentally demonstrated the capability of controlling nonlinear system parameters by performing open loop measurements below threshold conditions for a range of values of the external phase parameter Δ. The corresponding drive amplitude sweeps are shown in Figure A14(b)-(d). Figure A14(b) shows the oscillator behavior with a negative effective Duffing coefficient, while Figure A14(d) shows a positive Duffing coefficient. At intermediate phases, the nonlinear constant vanished and the viscous damping was increased, which was evident from the increased peak widths at higher drive levels, shown in Figure A14(c).

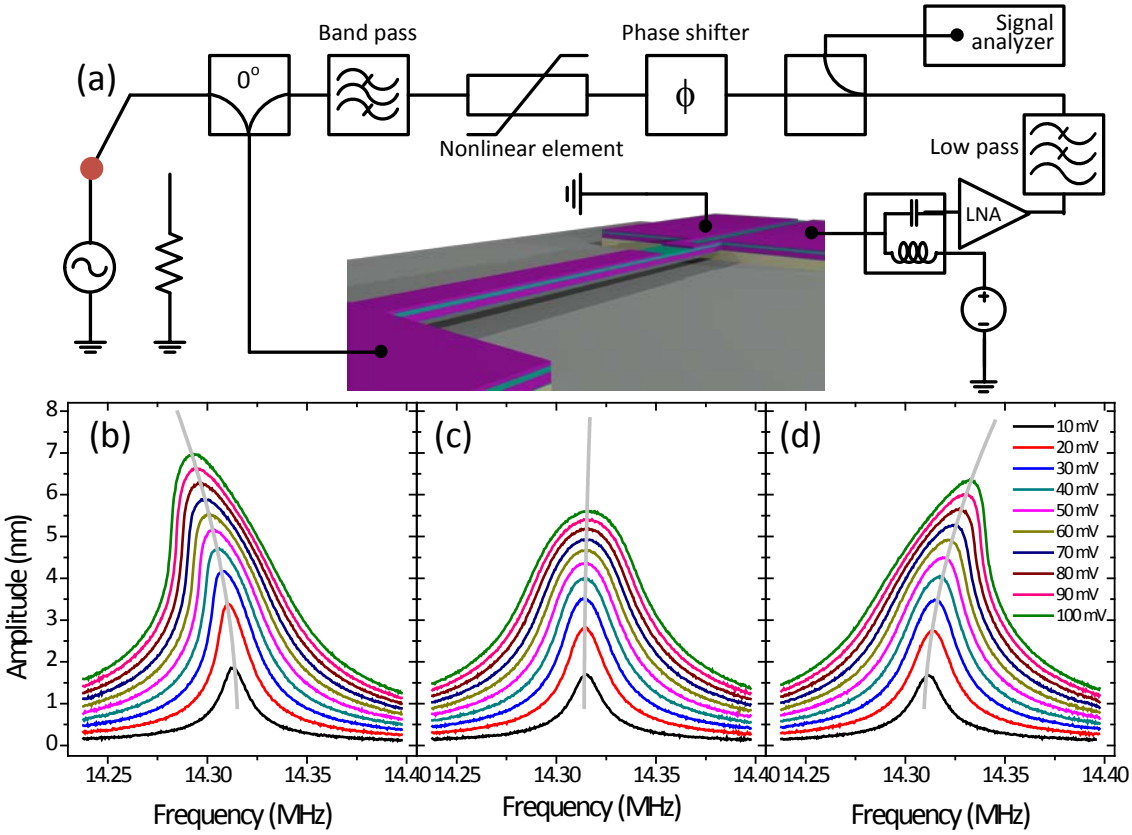

Figure A14: (a) Schematic of the Parametric feedback Oscillator implementation (b)–(d) Amplitude sweeps taken at different values of the External Phase Δ, where the Resonator had effective Negative (b) and Positive (d) Nonlinear Coefficients (c) the Nonlinear Coefficient vanished while the effective viscous damping was increased

When the threshold condition for oscillation is met and the motion is kick started with an external drive, the oscillator entered self-sustained oscillations. The comparison between the normalized open loop network analyzer scan and a spectrum of the closed loop parametrically fed back nonlinear oscillator is shown in Figure A15(a). We observe a change in the effective quality change from ~1200 to ~99000, corresponding to a compression ratio of 82.

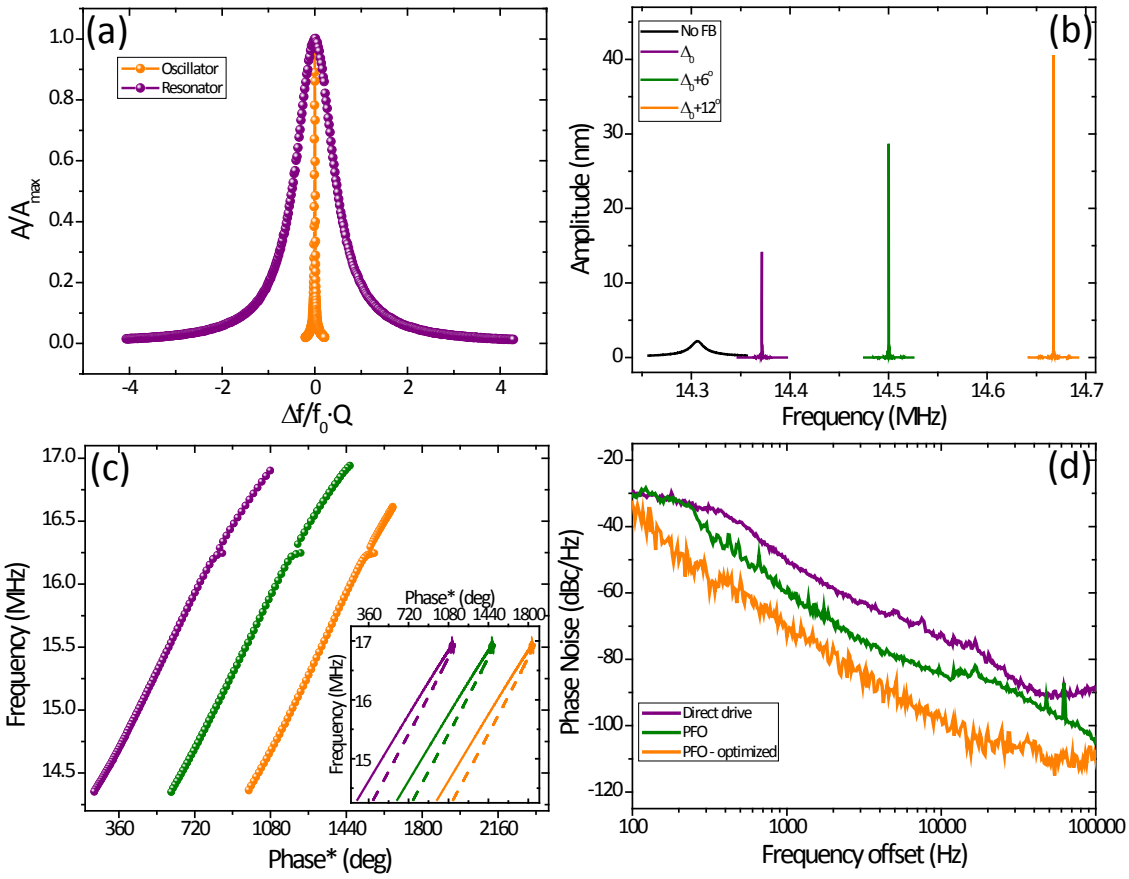

Figure A15: (a) Spectral measurement of the Oscillator (orange) in comparison with the Resonator (magenta) frequency sweep, showing a factor of ~82 compression ratio (b) Spectra of self-sustained Oscillations taken at three different external Phases (the linear resonator Lorentz curve is shown in black for comparison) (c) Dependence of the frequency on the external Phase (Three branches separated by 360^o are shown, and the flattening feature is evident in each. The inset shows the theoretical prediction: solid lines are the stable and dashed the unstable solution branches) (d) Phase noise comparison(typical parametric feedback phase noise is shown in green, the phase noise near the flattening point is shown in orange, and the direct drive oscillator phase noise is shown in magenta)

The theoretical analysis of the dynamical equation of the parametrically fed back oscillator predicts a strong dependence of the frequency and amplitude of oscillation on the external phase parameter. Figure A15(b) shows the spectrum analyzer measurements taken at different external phase parameters. The original network analyzer measurement is shown in black for comparison. We measured the frequency of oscillation while gradually varying the external phase, by means of the voltage controlled phase shifter. We show the results of this measurement in Figure A15(c). It can be observed a range of tunability of the order of 12% (14.5 to 17 MHz), which is extremely valuable for applications such as voltage control oscillators, external temperature or vibration compensation, and synchronization of coupled oscillators. The phase range accessible in our experiment was more than 1000^o; we therefore were able to observe three different solution branches of stable oscillation separated by 360^o, as shown in Figure A15(c). The measurements agree well with the theoretical prediction shown in the inset of Figure A15(c).

A more detailed analysis of the experimental results reveals a flattening of the frequency versus phase plot occurring at ~16.2 MHz in all three existence branches. We attribute this feature to the presence of an in-plane vibration mode (expected to be at ~32.4 MHz from finite element modeling) which is directly driven by the feedback signal. Thus, the wide tuning range in our oscillators allows the possibility of coupling widely separated modes.

In order to characterize the performance of the oscillator we performed phase noise measurements. We found that phase noise characteristics did not significantly change with the external phase parameter except for the flattening feature at 16.2 MHz. In Figure A15(d), the typical phase noise of a parametrically fed back oscillator is shown in green, and the phase noise at the flattening feature is shown in orange. These experiments demonstrated that the phase noise performance of our parametric feedback oscillator was superior to a direct drive oscillator based on the same NEMS resonator.

A.4.2 High Frequency Demonstration

An important goal is to scale these devices to higher frequencies. To implement this we fabricated a new run of the parametric resonators scaled down to ~4 μm in size and up to ~100 MHz in frequency. A resonator of such small dimensions suffered from poor transmission characteristics. The feed-through or cross talk signal, which manifested itself as an RF background, was much larger than the useful motion signal. The open loop resonance measurement with off-chip components is shown in Figure A16(a). Alternatively, we measured the same open loop resonance response with a printed circuit board developed in collaboration with our industrial partner Rockwell-Collins. We plot the result in Figure A16(b). The insets in each plot show zoomed plots that indicate the mechanical signal.

A transfer function such as shown in Figure A16 is impractical for building a traditional direct drive oscillator, since it is challenging to filter out the mechanical signal so that it alone met the Barkhausen criterion and a careful background cancellation should be performed (as already described). Otherwise, an attempt to build an oscillator would inevitably create multiple spurious oscillations due to the high RF feed-through levels. However, we showed that it is possible to sustain mechanical oscillations by means of our novel parametric feedback oscillator scheme.

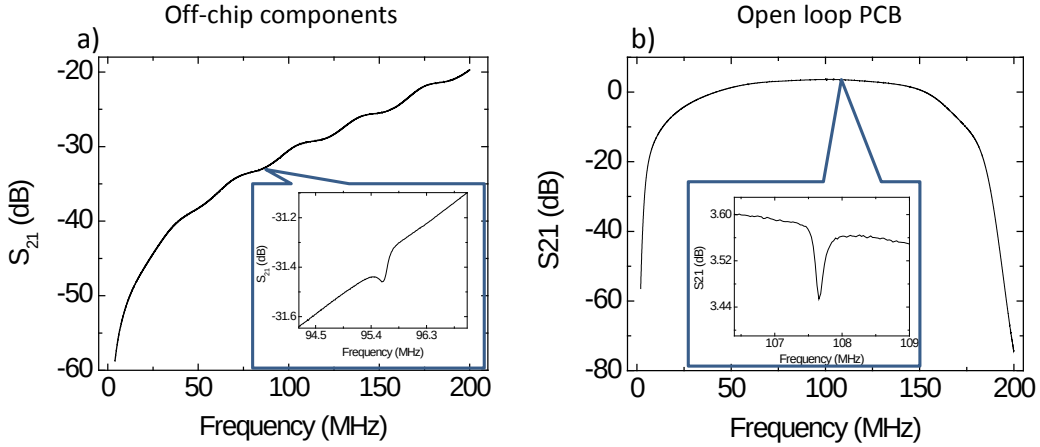

Figure A16: (a) Open Loop measurement of very high frequency (VHF) Resonator with Off-chip Components (b) Open Loop measurement of VHF Resonator with Rockwell's Printed Circuit Board (PCB)

The insets in each plot indicate the mechanical signal.

In order to do so, we built a circuit similar to the one described previously. The transduction used was the already described piezoelectric-piezometallic, and then it was passed through a nonlinear element to generate the 2ω harmonic. The 2ω signal proportional to the square of the mechanical motion was then filtered, phase shifted, adjusted in amplitude, and applied to the parametric input of the resonator. Thus, oscillations at ω were parametrically excited. Due to the large frequency separation of actuation and detection signals it is possible to obtain mechanical oscillation despite excessive, otherwise prohibitive, crosstalk characteristics.

An example of a spectrum analyzer measurement of the operating PFO is shown in Figure A17(a). The phase noise measurement for such operating point is shown in Figure A17(b) (purple), together with the expected thermomechanical limit (orange). We demonstrated a phase noise of -66dBc/Hz @ 1kHz offset for the 106 MHz resonator, indicating substantial improvement compared to our previous demonstration in the HF band. The demonstrated performance was still above the thermally limited phase noise as shown in Figure A17(b), indicating room for potential improvement.

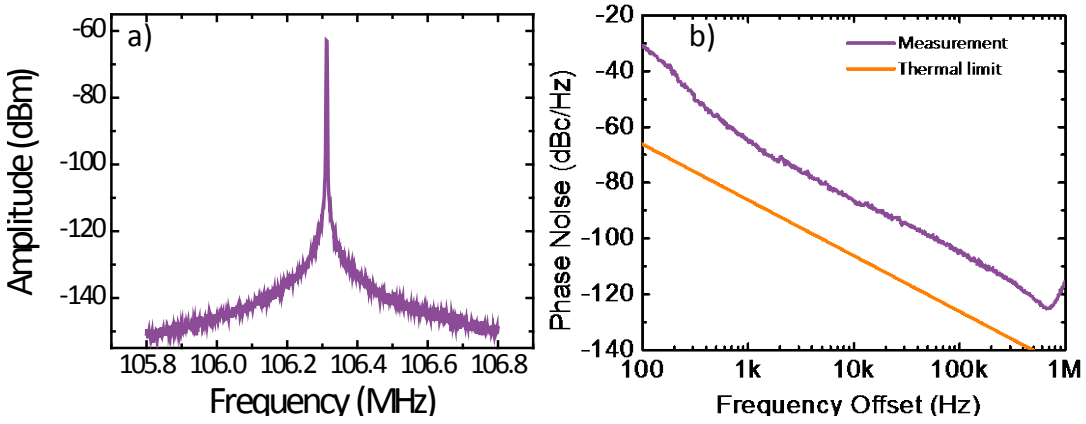

Figure A17: (a) Spectrum Analyzer measurement of operating VHF PFO (b) Example of Phase Noise measurements of the Parametric Feedback Oscillator
Thermal noise limited performance is shown as the orange line in this plot.

We also investigated the behavior of the VHF-PFO as a function of external feedback phase. We observed large tunability of the frequency as plotted in Figure A18(a). The phase noise measured at 1kHz offset is shown in Figure A18(b). It is possible to see a trend of improvement of the phase noise, consistent with the observation of the magnitude of oscillation, which continuously increases in the same range of external phase, as shown in Figure A18(c).

We thus successfully demonstrated VHF-PFO operation despite detrimental S_{21} transmission characteristics. We were able to build the PFO feedback circuit not only out of off-chip components in an academic setting, but also using printed circuit boards developed in collaboration with Rockwell-Collins.

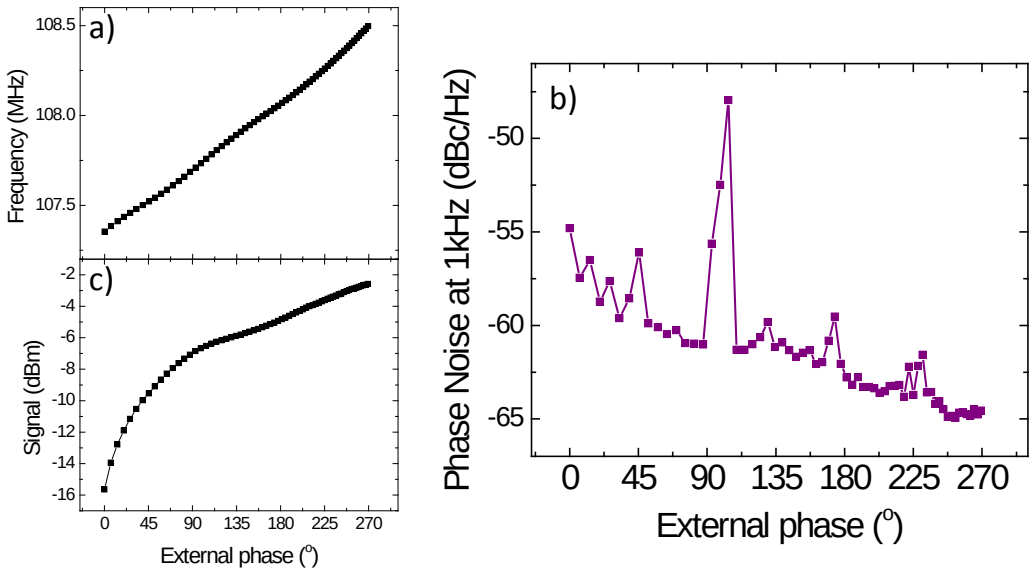

Figure A18: (a) Dependence of the frequency of PFO Oscillation on the external feedback Phase (b) Phase Noise at 1kHz measured at different external Phases (c) Magnitude of the Oscillations as a function of external Phase

APPENDIX B - MAJOR THEORETICAL ACCOMPLISHMENTS IN PHASE I

B.1 Envelope Formalism Approach

The envelope formalism analysis approach is based on the assumption that the system's dynamics is composed of several time scales. For NEMS oscillators, the most obvious two are the oscillation period, dictated by the resonant frequency of the beam ω_0, and the transient decay time, set by the resonator's quality factor Q. Expressing the oscillations as $q = A(T)e^{i\omega t} + c.c.$, with slow time $T \ll t$, allows us to separate the dynamics of the two time scales, and analyze the oscillator performance by focusing on the phase of the slow envelope $\phi = -i\arctan\big(Im(A)/Re(A)\big)$. In the presence of white noise sources of intensities I_n, and long after transients have decayed, this analysis provides us with the phase diffusion of the limit-cycle oscillator, which is linearly growing in time according to Eq. (5):

$$\langle[\phi(T+\tau) - \phi(T)]^2\rangle = \sum_n I_n D_n |\tau| \tag{5}$$

The diffusion coefficients D_n can be interpreted as the proportionality coefficient between the noise in a parameter controlling the oscillator operation and the oscillator's phase noise. They are defined as the square scalar product of two vectors: $D_n = (\vec{v}_\perp \cdot \vec{v}_n)^2$. $\vec{v}_n$ is the noise vector, and represents the modulation of the noise intensities with the oscillation signal. The vector $\vec{v}_\perp$ captures the phase sensitivity of the system, through the Jacobian matrix describing the linearized flow in the vicinity of the limit-cycle. Specifically, it is the eigenvector of the transposed of this Jacobian matrix that corresponds to the zero eigenvalue.

B.1.1 Non-stationary and Colored Noise

An actual oscillator circuit contains non-stationary noise sources because the noise is modulated by the signal as it goes through the amplifier. This makes the noise cyclo-stationary with the periodicity of the signal. However, since the oscillator is driven by its own feedback signal rather than by an external periodic source, it possesses a phase invariance property. Therefore, the oscillator's fundamental characteristics should be invariant to a time translation, and its output should be a stationary stochastic process. Also, the typical noise sources in oscillators with electrical feedback loops are colored; being affected by, for example, 1/f noise.

To extend the analysis to non-stationary and colored noise sources, we need to examine how the noise translates from the underlying equations of motion to the slow envelope dynamics centered around the resonant frequency. Expressing the noisy signal as $q + \xi$, where $q(t)$ is the deterministic signal and $\xi = \Xi(T)e^{i\omega t} + c.c.$ is random noise with correlation $\langle\xi(t)\xi(t')\rangle = f(t,t')$, allows us to derive the correlations in the amplitude formalism, and show that even for noise which is cyclo-stationary in the fast time scale, the leading order correlation in the slow amplitude formalism remains stationary $\langle\Xi(T)\Xi(T')\rangle = F(T-T')$. The phase variance $\langle[\phi(T+\tau) - \phi(T)]^2\rangle$, which depends on the noise correlation and the intrinsic sensitivity, can then be obtained for white and $1/f$ noise. This provides a comprehensive analysis of oscillator phase noise, and exposes its dependence on circuit elements such as amplifiers or filters.

B.2 Optimal Operating Points of Oscillators Employing Nonlinear Resonators

B.2.1 Parameter Noise

As stated above, calculating the zero mode of the transposed Jacobian matrix provides the phase diffusion that results from any white noise vector acting on a circular limit-cycle. However, if the noise originates from fluctuations in some parameters p_n of the equations, the diffusion coefficient can be shown to be the squared derivative of the scaled oscillation frequency with respect to the noisy parameter: $D_n = (d\Omega/\, dp_n)^2$. This representation of the diffusion coefficient reveals that if the frequency Ω is locally unchanged by p_n, the phase is unaffected by noise in p_n. This principle can be applied to reduce the phase noise of an oscillator based on a nonlinear resonator. To demonstrate this, we consider an oscillator composed of a nonlinear resonator whose motion is transduced and amplified to a heavily saturated value S, phase shifted by Δ, and fed back to sustain the motion. Analyzing the oscillator in the amplitude formalism shows that the amplitude of oscillation as a function of the scaled oscillation frequency Ω is given by the well-known Duffing curve, which is plotted in Figure B1(a).

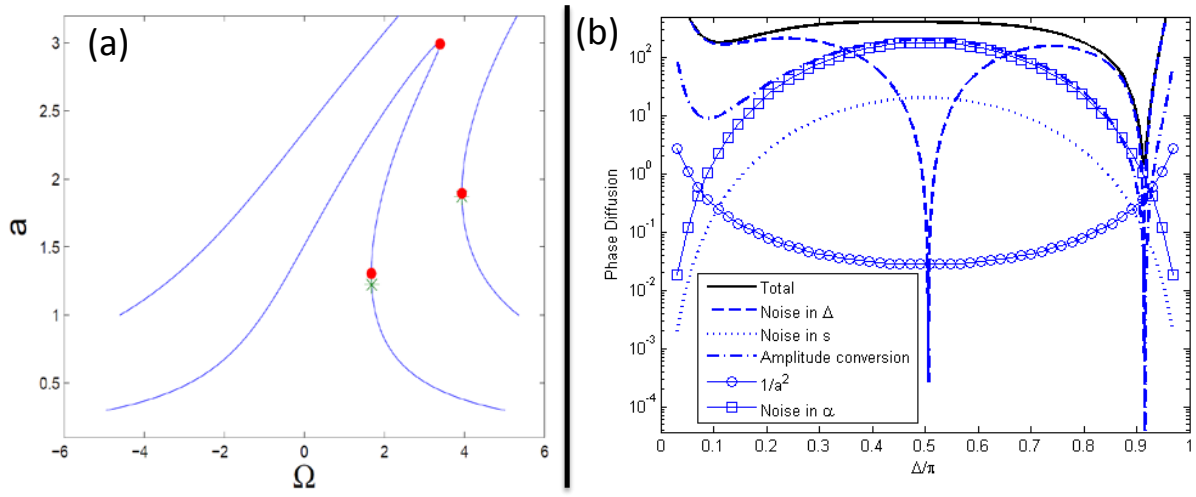

Figure B1: (a) The amplitude of Oscillation vs. Oscillation Frequency (both quantities scaled) for a Duffing type heavily-saturated Oscillator (The red dots (Yurke points) satisfy $d\Omega/d\Delta = 0$ (incidentally, also $d\Omega/da = 0$) and eliminate noise in Δ. The green stars (Kenig points) satisfy $\partial\Omega/\partial a = 0$ and eliminate the amplitude-phase noise conversion) (b) Particular example (for $S = 6$) of the calculated contributions to the Phase Diffusion Coefficient (proportional to phase noise) from noise in different Parameters as a function of the feedback Phase Parameter, Δ (both Yurke points are evidenced by sharp drops in the term "noise in Δ". Kenig point is also clearly shown by a sharp drop in the "amplitude conversion" term)

The two red points on the curve are the already mentioned Yurke points, for which $d\Omega/da = 0$, which in this case necessarily implies that they also satisfy $d\Omega/d\Delta = 0$. The implication of this is that at these points, noise in the feedback phase Δ has no effect on the oscillator's phase diffusion. This result, as already introduced above, is a generalization of the understanding of Yurke *et al.* who showed that if the resonator is operated at the critical Duffing point (where the two red dots merge into one), the noise in the phase of the feedback signal has no effect on the oscillator phase noise. In

Figure B1(b), dashed blue curve, the coefficient D_Δ versus phase Δ for a given value of S can be seen, with two sharp drops corresponding to both Yurke points.

It is also possible to monitor the phase diffusion that results from noise in the saturation level S, $D_S = (d\Omega/ds)^2$, indicates that at the top red point D_S increases as a function of S, and at the bottom red point it decreases as a function of S. Therefore, operating at the bottom point and increasing the saturation level, it is possible to minimize the contributions of noise in S and Δ, thus canceling the noise in both the real and imaginary quadratures of the feedback signal.

Operating points that satisfy $d\Omega/d\Delta = 0$, therefore suppressing the contribution to the oscillator's phase noise caused by noise in the feedback phase, exist not only for a directly driven oscillator, but also for a parametrically driven oscillator. In addition to the maximums of each predicted existence branch shown in Figure A14(c)-inset, the experimental curves also feature local plateaus, i.e. flattening features in Figure A14(c). These features are successfully modeled as coupling to another mechanical mode, which extracts energy from the parametric mode and flattens the amplitude and frequency response to the phase Δ. These flat regions are more accessible experimentally than the maximums, since the latter are close to the instability points (saddle nodes). Operating at those points also reduces phase noise, as shown in Figure A14(d).

B.2.2 Amplitude-phase Detachment

In the case of a nontrivial dependence of the frequency on amplitude, the term $\partial\Omega/\partial a$ multiplies the noise contributions in the amplitude quadrature to transform them into the phase quadrature. Therefore, operating points that satisfy $\partial\Omega/\partial a = 0$ (a.k.a. Kenig points) eliminate the amplitude-phase noise conversion. This cancels the effect of additive thermal noise from the amplitude quadrature, and since damping terms (that are generally linear and nonlinear) appear only in the dynamical equation for the amplitude, the effect of noise in the damping coefficients is eliminated as well. The points satisfying the amplitude-phase detachment condition $\partial\Omega/\partial a = 0$ are noted in Figure B1(a) as green stars. In Figure B1(b), the diffusion coefficients proportional to $\partial\Omega/\partial a$ can be seen in a blue dash-dotted line.

Note that on the upper curve in Figure B1(a), which is plotted for a higher saturation level, Kenig point approaches the bottom Yurke point. As a result, operating in the vicinity of Kenig point and increasing the saturation level of the amplifier as much as possible, would minimize the contribution of the noise in the feedback phase Δ, the saturation level S, and the amplitude-phase noise conversion. Thermal noise in the phase quadrature is also minimized because it is inversely proportional to the square of the oscillation amplitude which grows as we increase the saturation level. This offers a dramatic improvement over other proposed operating points, such as the original Yurke point for drive at the critical amplitude, $\Delta = 2\pi/3$, which only eliminates noise in Δ. Experimental verification of these predictions can be seen in Figure A9.

B.3 Theoretical Work on Anomalous Phase Noise

Due to the importance, already mentioned before in section A.3-(d), of the Anomalous Phase Noise, a great effort concentrated on understanding the sources of direct phase fluctuations, and ways of identifying and characterizing these fluctuations. Such fluctuations are induced by frequency noise and, as mentioned before, methods for suppressing the effects of this noise in NEMS are not currently known. Therefore, for successful development of NEMS-based oscillators it is critical that designers be able to measure this noise and identify its sources.

An important source of frequency noise in NEMS is random attachment and detachment of molecules to the resonator. This leads to fluctuations of the resonator mass and, as a consequence, its frequency. We developed a general method of describing spectral broadening from discrete frequency jumps. This method is based on studying coupled partial susceptibilities of the resonator, and it provides new insights into the problem of dephasing. Specifically, it allows one to follow the evolution of the spectrum from the well-resolved fine structure that occurs for comparatively large and rare jumps, to the broadened single peak that corresponds to small and frequent jumps, or to a large number of states with different frequencies. The spectrum of a nanoresonator with attaching and detaching molecules (or nano-particles) was found in explicit form, and its sensitivity to system parameters was analyzed. The evolution of the spectrum with varying parameters of the attaching molecules is shown in Figure B2.

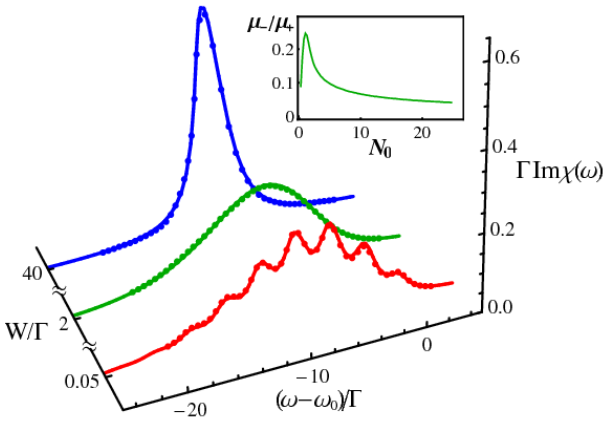

Figure B2: Absorption Spectrum of the Resonator Imχ with attaching and detaching Molecules for different attachment Rates

W scaled by the oscillator decay rate Γ; ω_0 is the resonator eigenfrequency. The average number of attached molecules is N_0=3, and the frequency change per molecule is $\Delta = 3\Gamma$. Data points show the results of numerical simulations. Inset: the asymmetry parameter as function of N_0 for $W/\Gamma = 2,\ \Delta/\Gamma = 3$.

We also studied the resonant response of an underdamped nanomechanical resonator with frequency fluctuations due to diffusion of molecules or microparticles along the resonator. Such diffusion leads to a broadening and a change in the shape of the oscillator spectrum. The spectrum was found for the case when the diffusion is confined to a small part of the resonator, as well as the case where the diffusion occurs along the entire nanobeam. The analysis was based on extending to the continuous limit, and appropriately modifying, the method of interfering partial spectra. The onset of characteristic double-peak spectra in the case where particles can diffuse over the entire nanobeam was predicted. We found general conditions where the only source of the spectral broadening is the effect of frequency fluctuations described by a convolution of the spectra without these fluctuations and with them. Estimates were obtained for the effects of this diffusion for important classes of nano-mechanical resonators.

An important new effect that can be caused by diffusion of massive particles along a nanoresonator is the onset of bistability of resonant response. The bistability can emerge even where the internal nonlinearity of the resonator is still small. The underlying mechanism of this new effect is the dependence of diffusion on the vibration amplitude through inertial effects, specifically the dependence of the resonator frequency on the distribution of particles along the beam. The

bistability can be seen if the diffusion coefficient D is sufficiently large. Interestingly, the diffusion is essentially noise, yet this noise can lead to a coherent nonlinear behavior. However, because of the nature of diffusion, the lifetime of the coexisting vibrational states is finite. It exponentially increases with increasing D and displays a scaling dependence on the parameters close to bifurcation points. The onset of bistability and the switching between the coexisting states is seen in Figure B3.

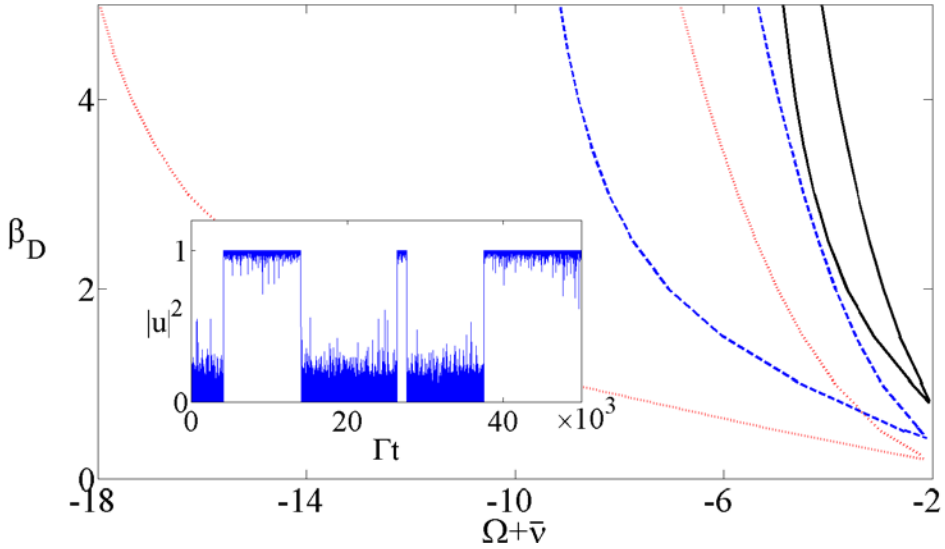

Figure B3: Regions of Bistability of a Nanoresonator with a Particle diffusing along it
Displayed in the parameter plane of the scaled intensity β_D and the detuning of the modulating field frequency ω from the resonator eigenfrequency ω_0. The solid, dashed, and dotted lines show pairs of bifurcation lines for different mass of the diffusing particle; the bistability occurs inside the corresponding wedges. The inset shows the simulated scaled squared amplitude of forced vibrations as a function of the scaled time in a bistability region.

We also developed an approach to separate and characterize frequency fluctuations in vibrational systems. In two-level systems, frequency fluctuations lead to the difference between the T_1 and T_2 relaxation times and are routinely separated from decay using nonlinear response to an external field. The nonlinear techniques do not immediately apply to linear vibrations, since their response is inherently linear, and much information is extracted from the spectrum of the response. We showed that frequency fluctuations of a resonator can be studied by using, in a different manner, essentially the same measurement as that used to find the absorption spectrum, i.e. by looking at the response of a modulated resonator. The idea is to study such correlators of the quadratures that are specifically sensitive to frequency fluctuations, in particular, correlators and moments of the complex vibration amplitude. These allow one not only to reveal frequency noise, but also to study its statistics and the power spectrum, for both classical and quantum vibrations, as can be inferred from Figure B4. The sensitivity to the noise statistics was illustrated for important examples of the noise.

We also developed a method for determining the statistics of parameter values at which a system will leave a metastable state as a system parameter is swept across a bifurcation value in the presence of noise. The distribution of the attendant amplitude jump events was obtained for small noise intensity relative to the appropriately scaled parameter sweep rate, but the results go beyond the standard adiabatic approximation, which significantly increases the accuracy of determining the bifurcation parameter value. This problem is directly relevant to the experimental determination of system parameters for nonlinear micro/nanoresonators.

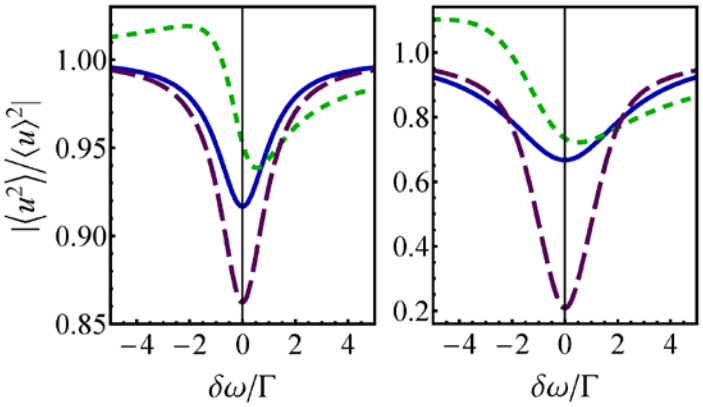

Figure B4: Scaled second moment of the Complex amplitude of forced Vibrations u as a Function of the detuning $\delta\omega$ of the driving Field Frequency from the Resonator Eigenfrequency

The solid, short-dash, and long-dash curves provide results for Gaussian, Poisson, and telegraph frequency noise, respectively. The left and right panels refer to the relative Gaussian noise intensities $D/\Gamma = 0.1$ and 1. For the Poisson noise we used unit pulse area and the same intensity as the Gaussian noise. For the telegraph noise we chose the switching rate D and the variance D^2.

B.4 A Passive Phase Noise Cancellation Element

The demonstrated ability to make the oscillator's phase be unaffected by noise in a parameter can also be used to create a passive phase noise cancelation element. A NEMS realization of such a device is illustrated in Figure B5(a). The device is made of a pair of coupled resonating elements that are parametrically-driven with a noisy frequency near the sum of their linear frequencies $\omega_1 + \omega_2$. It produces a signal with reduced noise at a frequency near the difference of these linear frequencies $\omega_2 - \omega_1$. The generation of signals at two frequencies by parametric excitation at the frequency sum is called nondegenerate parametric response, a phenomenon that has been mostly studied in the context of optical parametric oscillators (OPOs). We theoretically demonstrate how it can be used to eliminate oscillator phase noise.

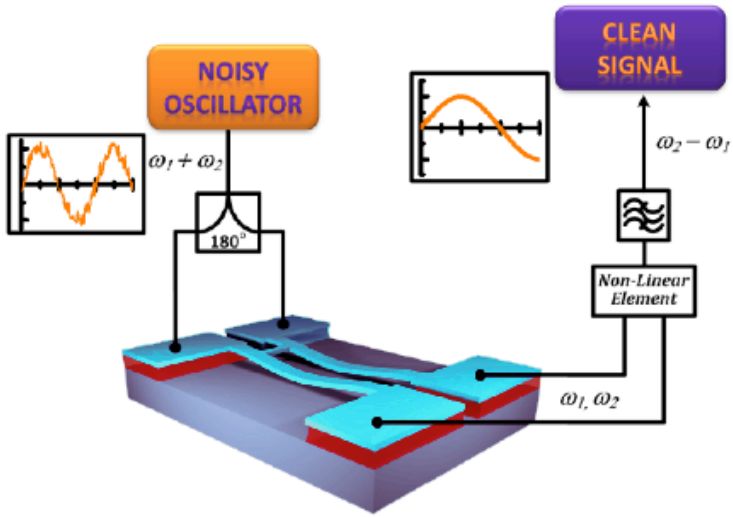

(a)

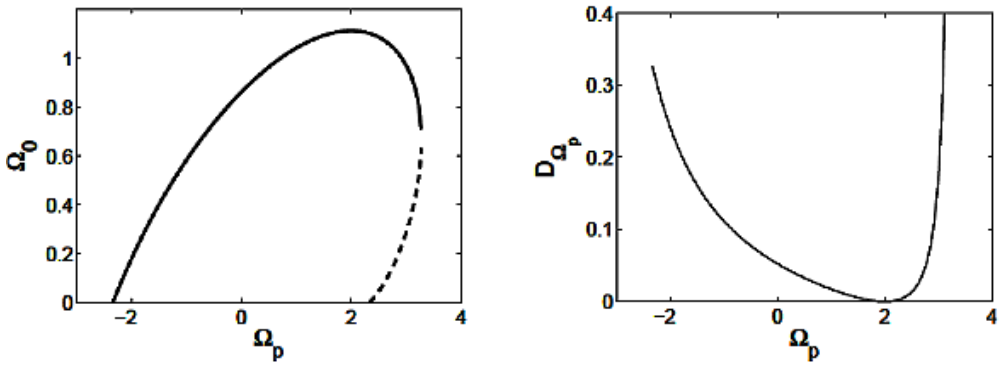

(b) (c)

Figure B5: (a) Illustration of the Phase Noise Elimination Scheme. An oscillator produces a signal with a noisy frequency around $\omega_1 + \omega_2$. This signal parametrically drives a pair of coupled beams with a relative phase of 180° to induce non-degenerate response. The output signal at a frequency around $\omega_2 - \omega_1$ is obtained by squaring and filtering. (b) Limit Cycle Oscillation Frequency as a function of the drive Frequency. Both quantities are scaled. (c) Phase Diffusion induced by Frequency Noise of Unit Strength. The phase diffusion coefficient is zero around $\Omega_p \approx 2$, and it is also smaller than the phase diffusion of the driving oscillator along most of the curve. The curve can be calculated as the squared derivative of the solid curve in (b).

A key result is that non-degenerate parametric oscillations are not locked to the driving source, and that the dynamics contains a phase-translation invariance that corresponds to the existence of a limit-cycle. Figure B5(b) shows the limit-cycle frequency as a function of the drive frequency. As the drive frequency Ω_p is swept, the limit-cycle frequency Ω_0 reaches a maximal value. Since at this maximum: $d\Omega_0/d\Omega_p = 0$, noise in Ω_p has no effect on the limit-cycle phase. This can be shown to correspond with making the output signal at frequency around $\omega_2 - \omega_1$ completely insensitive to noise in the drive frequency, which provides a method to clean phase noise of the driving oscillator. It is also noteworthy that for the parameters used to plot the diffusion coefficient $D_{\Omega_p} = \left(d\Omega_0/d\Omega_p\right)^2$ in Figure B5(c), the frequency stability is also improved along most of the curve,

since $D_{\Omega_p} < 1$ (output frequency noise less than input frequency noise), indicating that this passive device could be broadly applicable to enhance the performance of existing oscillator designs.

B.5 Theoretical Efforts by MSU Team

The efforts by the MSU team on the DEFYS project consisted of several activities related to advancing fundamental understanding of phase noise mechanisms and to developing tools and strategies for reducing phase noise in oscillators.

We considered phase noise in oscillators employing nonlinear frequency selective elements. Our treatment of this problem is outlined as follows. Our assumptions include neglecting the dynamics of the feedback loop and treating the resonator as nearly conservative. We employ action-angle coordinates for the model and consider the closed loop dynamics of a general nonlinear closed loop oscillator. Our primary result is an expression for the spectrum of fractional frequency fluctuations in the oscillator. This expression is useful for oscillator tuning and optimization. We illustrate this by examining an oscillator employing a biased Duffing resonator. Using noise and damping effects developed from a microscopic noise/dissipation model and a simple feedback model, we consider oscillator tuning by varying the bias and the amplitude of oscillation. It is found that the minimum phase diffusion rate occurs where the frequency of the resonator is locally independent of the amplitude, the so-called sweet spot. Tuning at this point minimizes the migration of amplitude noise into phase noise. A reduction in phase noise of 5 decibels is achieved by tuning at this point. Details of this analysis are presented in the thesis of Miller. This analysis sets the stage for extensions, which include the following:(i) design of devices that allow for tuning to the sweep spot, for example, by using electrostatic bias or other symmetry lifting mechanisms in micro-resonators; (ii) consideration of shaping the underlying limit cycle to minimize the phase noise. This can be achieved by device design, but the details depend on the nature of the noises acting in the system; (iii) consideration of using nonlinear coupling to secondary modes to reduce phase noise of the mode of interest. This effect has been observed experimentally by groups at Caltech and Argonne and the analysis in Miller's work can be extended to analyze these systems and provide a basis for systematic design of coupled mode devices.

We investigated an intrinsic limitation on the phase noise of the oscillator, specifically that imposed by frequency fluctuations of the resonator itself. We have identified new mechanisms of frequency fluctuations and studied their effect on the response of the resonator to external driving. We have also developed means for revealing the very presence of frequency fluctuations and characterizing them, including determination of their intensity and statistics. The analysis was based on combining the method of averaging of nonlinear dynamics with the techniques of the theory of random processes, the adiabatic approximation technique, and other techniques of nonlinear dynamics and theoretical physics.

Specifically, we have studied an underdamped oscillator with random frequency jumps. We described the oscillator spectrum in terms of coupled susceptibilities for different-frequency states. Depending on the parameters, the spectrum has a fine structure or displays a single asymmetric peak. For nanomechanical resonators with a fluctuating number of attached molecules, it is found in a simple analytical form. The results bear on dephasing in various types of systems with jumping frequency. The proposed mechanism has been already used to describe the hitherto mysterious effect of the sharp increase of the width of spectral peaks of atomic force microscopy (AFM) resonators as they are brought close to a surface.

We also considered frequency fluctuations of an underdamped nanomechanical resonator due to diffusion of molecules or microparticles along the resonator. They lead to broadening and change of shape of the oscillator spectrum. The spectrum is found for the diffusion confined to a small part of the resonator and where it occurs along the whole nanobeam. The analysis is based on extending to the continuous limit, and appropriately modifying, the method of interfering partial spectra. We established the conditions of applicability of the fluctuation-dissipation relations between the susceptibility and the power spectrum. We also found where the effect of frequency fluctuations can be described by a convolution of the spectra without these fluctuations and with them as the only source of the spectral broadening.

We found an unexpected and nonintuitive effect of frequency fluctuations due to diffusion of absorbed particles along a nanoresonator. The diffusion depends on the vibration amplitude through inertial effect. We found that, if the diffusion coefficient D is sufficiently large, the resonator response to periodic driving displays bistability. The lifetime of the coexisting vibrational states exponentially increases with increasing D and displays a scaling dependence on the parameters close to bifurcation points.

We showed how frequency fluctuations of a vibrational mode can be separated from other sources of phase noise. The method is based on the analysis of the time dependence of the complex amplitude of forced vibrations. The moments of the complex amplitude sensitively depend on the frequency noise statistics and its power spectrum. The analysis applies to classical and to quantum vibrations.

We studied the effect of nonlinearity in nanoresonators based on carbon nanotubes. Nanotubes behave as semi-flexible polymers in that they can bend by a sizeable amount. When integrating a nanotube in a mechanical resonator, the bending is expected to break the symmetry of the restoring potential. We developed a new detection method that allowed us to demonstrate such symmetry breaking. The method probes the motion of the nanotube resonator at nearly zero-frequency; this motion is the low-frequency counterpart of the second overtone of resonantly excited vibrations. We find that symmetry breaking leads to the spectral broadening of mechanical resonances, and to an apparent quality factor that drops below 100 at room temperature. The low quality factor at room temperature is a striking feature of nanotube resonators whose origin has remained elusive for many years. Our results shed light on the role played by symmetry breaking in the mechanics of nanotube resonators.

We used a modulated resonator to study quantum fluctuations far from thermal equilibrium. A simple but important nonequilibrium effect that is encountered in modulated resonators is quantum heating, where quantum fluctuations lead to a finite-width distribution of the resonator over its quasienergy (Floquet) states. We have discussed the recent observation of quantum heating. We analyzed large rare fluctuations responsible for the tail of the quasienergy distribution and switching between metastable states of forced vibrations. We found the most probable paths followed by the quasienergy in rare events, and in particular in switching. Along with the switching rates, such paths are observable characteristics of quantum fluctuations. As we show, they can change discontinuously once the detailed balance condition is broken. A different kind of quantum heating occurs where oscillators are modulated nonresonantly. Nonresonant modulation can also cause oscillator cooling. We have discussed different microscopic mechanisms of these effects.

APPENDIX C - MAJOR ACCOMPLISHMENTS IN PHASE IB

C.1 Summary

In Phase I of this DEFYS Program, we developed the critical experimental and theoretical underpinnings for our effort towards high-frequency, low-phase-noise nonlinear NEMS oscillators. Following this was a transitional effort, Phase IB, wherein we adapted our techniques to a new class of NEMS devices which would allow us to significantly improve our phase noise and frequency performance. This has required significant changes in NEMS design and materials, and while we have made progress on this front, unexpected challenges in fabrication and test have delayed our realization of the next generation of NEMS oscillators to beyond the endpoint of the DEFYS program

C.2 Experimental Accomplishments

In our proposal for Phase IB of DEFYS program, we outlined that the experimental effort will be focused on circular nanomembrane oscillators. Our preliminary experimental investigations made at the end of Phase I yielded high performance resonators operating at 200MHz and higher. We determined that Piezoelectric-Piezoelectric (PZE-PZE) detection produced a large enough signal that nonlinear oscillation should be feasible. We, therefore, set up a new fabrication run focused on PZE-PZE nanomembrane resonators at the outset of Phase IB. However, the material used in Phase I had been exhausted, so we had to purchase new from a commercial provider, rather than getting it from our long term collaborator. Over the Phase IB timeframe, we have managed to finish several fabrication run and have tested the devices. The SEM images of some example devices are shown in Figure C1.

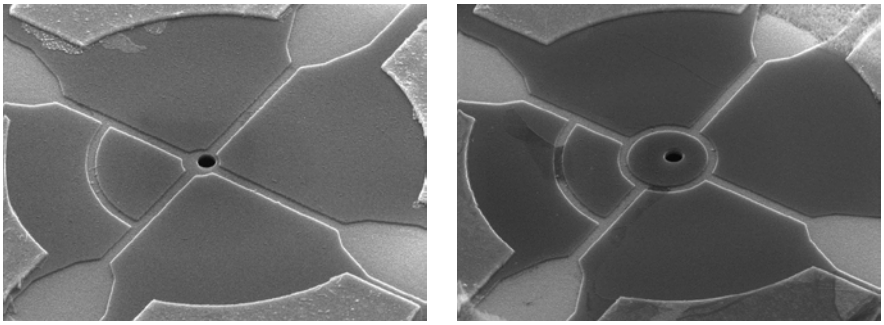

Figure C1: SEM Images of the Nanomembrane Resonator fabricated within the Phase IB Effort

As we were anticipating, the downside of such transduction technique – large RF cross-talk – hindered our ability to build an oscillator. Nevertheless, we utilized our proposed background cancelling technology by means of dummy bridge electrode on the same chip and managed to substantially reduce background. The schematic of the measurement and the experimental data for the resonance driven into the nonlinear regime are shown in Figure C2.

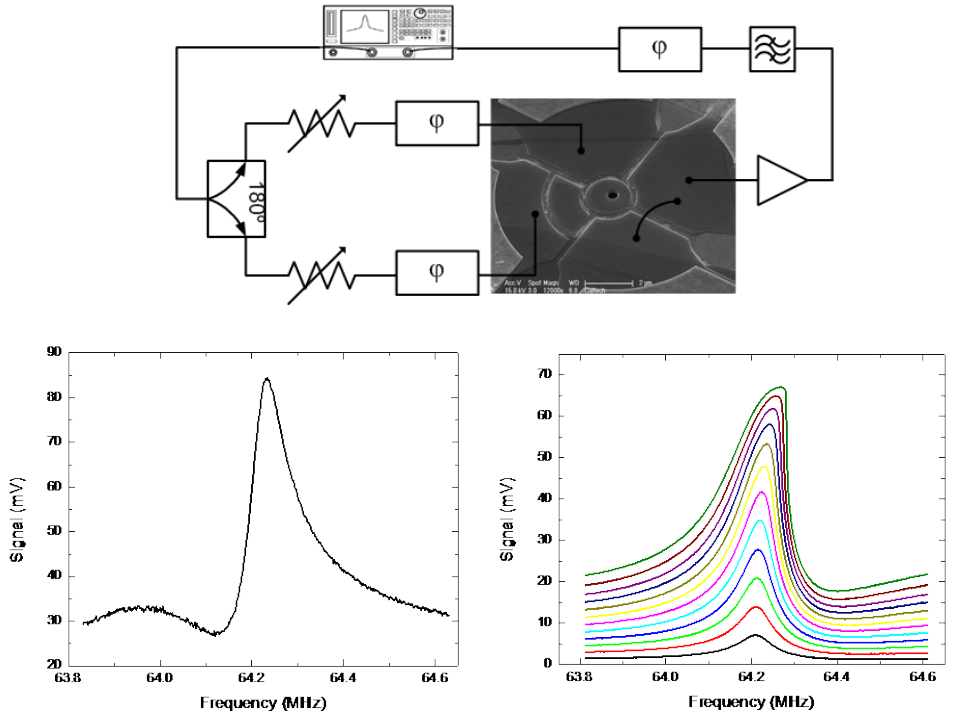

Figure C2: Measurement Schematic and First Experimental Data of the 2nd Generation Nanomembrane Resonator

After careful adjustment of the parameters of the bridge, we managed to satisfy the Barkhausen criterion and built the first ever NEMS PZE-PZE nanomembrane self-sustained oscillator. The spectral measurement and phase noise are shown in Figure C3. We observed the performance of -65 dBc/Hz at 1 kHz offset in this first non-optimized attempt.

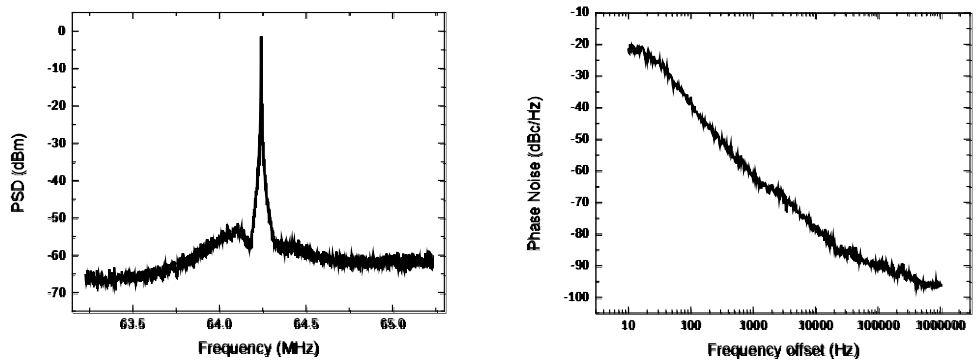

Figure C3: Spectral measurement of the Nanomembrane based self-sustained Oscillator and its Phase Noise Data

The quality of this new commercial material turned out to be poorer than the one we used previously; therefore, the achievement of PZE-PZE nonlinear oscillator at higher frequencies with this material will be more challenging. In order to address this problem, we reinitiated our close collaboration with our original provider and managed to get hold of world's first ultrathin aluminum nitride stack with the active layer thickness of 15 nm. We also requested this material be grown on sapphire in order to minimize RF crosstalk. After these wafers were delivered, however, we discovered additional challenges concerning the ultrathin layers, as conductive shorts across the

ultrathin PZE has led to vastly reduced signal and increased crosstalk. Moreover, these new wafers utilized platinum rather than molybdenum as the conducting layers, which has necessitated the development of new fabrication procedures for the membrane NEMS. In light of these challenges, we and our collaborator have decided to pursue an additional wafer run incorporating thicker AlN layers. While work on this is ongoing, we did not successfully make oscillator devices from this new material by the end of this Program; we expect new devices to be made and tested in 2014.

In parallel, we have fabricated 3rd generation nanomembranes made out of the traditional commercial wafer where we have utilized our well-developed piezoresistive readout scheme. We also plan to build high frequency oscillators out of these devices.

C.3 Theoretical Accomplishments

Theoretical accomplishments in Phase IB fall into three areas: analysis of the nonlinear behavior of circular membrane resonators in support of the Phase IB and future experimental work; generalizing the previous analysis of noise reduction strategies to feedback systems in which the amplifier is unsaturated; and new results for the elimination of 1/f noise.

With undergraduate researcher Chris Gong we analyzed the nonlinear behavior of circular membrane resonators. As well as routine calculations of the nonlinear behavior of individual modes, demonstrating the feasibility of transitioning from the beam to membrane oscillators, a particular focus of the work was to exploit the new possibilities raised by the mode degeneracies of the circular membrane, for example the m=+1 and m=-1 azimuthal modes. Following the analysis of Yeo and Lee [J. Sound Vibr. 257, 653 (2002)] Gong developed code to calculate the mode response in the open-loop driven configuration. An example is shown in the Figure C4 below.

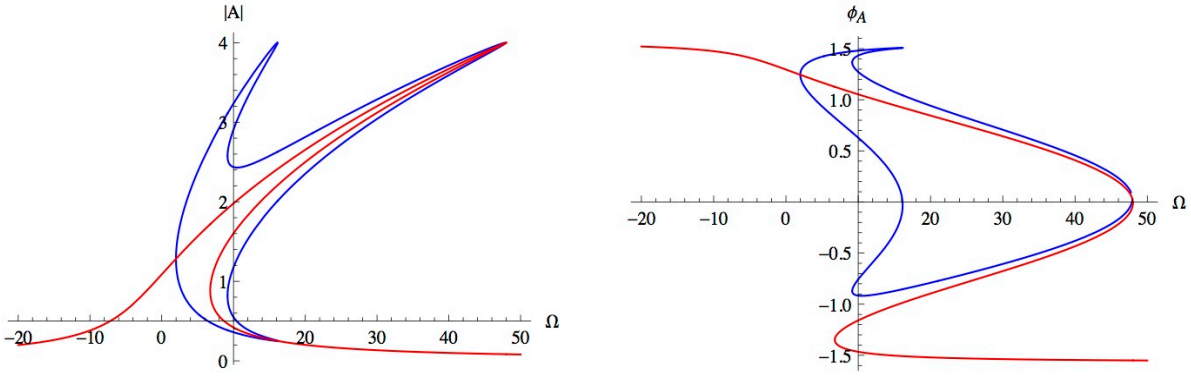

Figure C4: Amplitude and Phase Response as a function of the frequency offset (scaled by the line width)

The competition between standing and traveling waves leads to a rich response - these figures correspond to the “Duffing curves” of the simple resonator - with a number of turning points that might be exploited in noise reduction schemes. Gong also developed a code to investigate calculate the closed loop behavior to verify that this rich behavior persists in the self-sustained oscillator and to calculate the stability of the solutions. In the closed loop situation nonlinear root finding methods are needed to calculate the oscillating solutions. Future work will make the method more systematic by using root following schemes such as the “Auto” code.

The methods we have developed to reduce oscillator noise using optimal operating points described above, and the previous work in the literature, have relied on using saturated amplifiers in the feedback loop. In collaboration with the HRL Laboratories DEFYS effort postdoc Eyal Kenig, supported by the Phase IB funds, and co-principal investigator Michael Cross explored oscillator noise reduction under more general conditions using an unsaturated amplifier. We found that indeed complete noise quenching only occurs when the system is operated in the high amplitude, fully saturated regime, which corresponds to the system previously studied, but that substantial phase noise reduction can be achieved away from this limit, even when the oscillator operates at amplitudes far below the critical point for bifurcations of the associated open-loop system. Going from a saturated to an unsaturated amplifier leads to two different effects. Firstly, since the drive on the resonator is no longer constant as parameters such as the phase of the feedback signal are changed, the closed-loop oscillator behavior is no longer simply related to the open-loop resonator response curves, and the optimal operating points are not given by the turning points of the resonator Duffing curve. Secondly, noise from the amplifier is no longer confined purely to the phase direction, since fluctuations in the magnitude of the drive are no longer quenched by the saturation: noise along a line in phase space can be quenched by tuning a single parameter to find optimal operating points, but a noise "ball" cannot be eliminated by tuning a single parameter. This work is published in a joint paper with K. Wiesenfeld and K. Moehlis. Figure C5 below shows the total feedback phase-noise as a function of the feedback phase-shift for different values of the amplifier gain, with large gain giving the saturated limit.

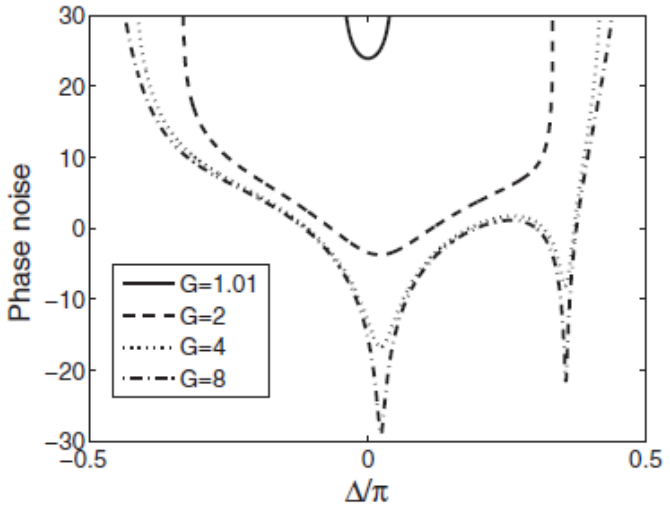

Figure C5: Total Feedback Phase-noise as a function of the feedback Phase-shift for different values of the Amplifier gain

Using our general method to analyze oscillators based on high-Q resonators in terms of an amplitude description of the resonator response formulated in Phase I, we discovered that for the particular case of 1/f noise sources (or, more generally, noise with a bandwidth small compared with the oscillator frequency) the noise in the feedback signal is always along a line in the amplitude phase space, rather than filling out a ball as is the case for other noise sources such as white noise (see previous paragraph). This unexpected result is based on a careful analysis of the projection of the cyclostationary amplifier noise onto the slow degrees of freedom of the resonator, which, because of the high-Q, acts as a strong filter of the high frequencies. This raises the possibility that 1/f noise can be quenched using the nonlinear properties of the resonator by tuning a single parameter even for the case of an unsaturated amplifier. A detailed analysis of particular 1/f noise sources and oscillator

configurations showed that this can indeed be accomplished. Since empirically feedback noise often is dominated by 1/f noise, and running the amplifier below saturation and without additional limiters in the circuit is likely to be improve the performance of the amplifier system, this is a very important result for the practical implementation of techniques to reduce or even eliminate the degradation of oscillator performance due to feedback noise. This work is written up in a paper submitted to Physical Review Letters.

APPENDIX D - PATENTS, PUBLICATIONS, AND PRESENTATIONS

D.1 Patent Applications

[1] Luis Guillermo Villanueva Torrijo, Rassul Karabalin, Matthew Matheny, Philip X.L Feng, Michael C. Cross, Michael L. Roukes, **"Parametric Feedback Oscillators"**, US Patent Application number 13/095,692.

[2] M. H. Matheny, R. B. Karabalin, L. G. Villanueva, Michael L. Roukes, **"Novel transduction technique to study NEMS nonlinearities"**, *Caltech Internal Application*, CIT-5794-P2.

[3] Eyal Kenig, M. C. Cross, Ron Lifshitz, R. B. Karabalin, L. G. Villanueva, M. H. Matheny, and M. L. Roukes, **"A passive phase noise cancellation element"**, *Caltech Internal Application*, CIT-6072-P, to be converted in January 2014.

[4] Matthew Matheny, Michael L. Roukes, Michael C. Cross, Luis Guillermo Villanueva Torrijo, and Rassul Karabalin, "**Synchronization of Nanomechanical Oscillators**", *Caltech Internal Application*, CIT 6358.

D.2 Publications (Scientific Journals)

[1] L.G. Villanueva, E. Kenig, R. B. Karabalin, M. H. Matheny, R. Lifshitz, M. C. Cross, and M. L. Roukes. *"Surpassing Fundamental Limits of Oscillators Using Nonlinear Resonators"*, **Physical Review Letters 110**, 177208 (2013).

[2] M. H. Matheny, L. G. Villanueva, R. B. Karabalin, J. E. Sader, and M. L. Roukes. *"Nonlinear Mode-Coupling in Nanomechanical Systems"*, **Nano Letters 13**, 1622-1626, (2013).

[3] L.G. Villanueva, R. B. Karabalin, M.H. Matheny, D. Chi, J. E. Sader, and M. L. Roukes. *"Nonlinearity in Nanomechanical Cantilevers"*, **Physical Review B 87**, 024304 (2013).

[4] E. Kenig, M. C. Cross, L. G. Villanueva, R. B. Karabalin, M. H. Matheny, R. Lifshitz, and M. L. Roukes. *"Optimal Operating Points of Oscillators Using Nonlinear Resonators"*, **Physical Review E 86**, 056207, (2012).

[5] E. Kenig, M. C. Cross, R. Lifshitz, R. B. Karabalin, L. G. Villanueva, M. H. Matheny, and M. L. Roukes. *"Passive Phase Noise Cancellation Scheme"*, **Physical Review Letters 108**, 264102, (2012).

[6] R. B. Karabalin, L. G. Villanueva, M. H. Matheny, J. E. Sader, and M. L. Roukes. *"Stress-Induced Variations in the Stiffness of Micro- and Nanocantilever Beams"*, **Physical Review Letters 108**, 236101, (2012).

[7] L.G. Villanueva, R. B. Karabalin, M.H. Matheny, E. Kenig, M. C. Cross, and M. L. Roukes. *"A Nanoscale Parametric Feedback Oscillator"*, **Nano Letters 11**, 5054-5059, (2011).

[8] M. I. Dykman, M. Khasin, J. Portman, and S.W. Shaw, *"Spectrum of an Oscillator with Jumping Frequency and the Interference of Partial Susceptibilities"*, **Physical Review Letters 105**, 230601 (2010).

[9] J. Atalaya, A. Isacsson, and M. I. Dykman, *"Diffusion-induced dephasing in nanomechanical resonators"*, **Physical Review B 83**, 045419 (2011).

[10] M. I. Dykman, M. Marthaler, and V. Peano, *"Quantum heating of a parametrically modulated oscillator: Spectral signatures"*, **Physical Review A 83**, 052115 (2011).

[11] Z. A. Maizelis, M. L. Roukes, and M. I. Dykman, *"Detecting and characterizing frequency fluctuations of vibrational modes"*, **Physical Review B 84**, 144301 (2011).

[12] J. Atalaya, A. Isacsson, and M. I. Dykman. *"Diffusion-Induced Bistability of Driven Nanomechanical Resonators*", **Physical Review Letters 106**, 227202 (2011).

[13] M. I. Dykman and I. B. Schwartz, *"Large rare fluctuations in systems with delayed dissipation:*, Phys. Rev. E **86**, 031145 (2012).

[14] N. J. Miller and S. W. Shaw, *"Escape statistics for parameter sweeps through bifurcations"*, *Physical Review E, **85***, 046202 (2012).
[15] A. Eichler, J. Moser, M. I. Dykman, and A. Bachtold, ``*Symmetry breaking in a mechanical resonator made from a carbon nanotube"*, Nat. Commun. **4**, 2843 (2013).
[16] V. Peano and M. I. Dykman, ``*Quantum fluctuations in modulated nonlinear oscillators"*, New Journal of Physics **16**, 015011 (2014)
[17] E. Kenig, M. C. Cross, J. Moehlis, and K. Wiesenfeld, "*Phase Noise of Oscillators With Unsaturated Amplifiers"*, arXiv:1310.7524, accepted for publication in **Physical Review E**.
[18] M. H. Matheny, M. Grau, L. G. Villanueva, R. B. Karabalin, M. C. Cross, and M. L. Roukes, "*Phase Synchronization of Two Anharmonic Nanomechanical Oscillators*", **Physical Review Letters 112**, 014101 (2014).
[19] E. Kenig and M. C. Cross, "*Eliminating 1/f Noise in Oscillators"*, **Physical Review E 89**, 042901 (2014).

Piezoelectric NEMS technology publications

[20] R. B. Karabalin, S. C. Masmanidis, and M. L. Roukes, *"Efficient parametric amplification in high and very high frequency piezoelectric nanoelectromechanical systems"*, **Applied Physics Letters 97**, 18, 183101 (2010).
[21] R. B. Karabalin, M. H. Matheny, X. L. Feng, E. Defay, G. Le Rhun, C. Marcoux, S. Hentz, P. Andreucci, and M. L. Roukes. *"Piezoelectric nanoelectromechanical resonators based on aluminum nitride thin films"*, **Applied Physics Letters 95**, 10, 103111 (2009).

D.3 Conference Contributions

[1] M. H. Matheny, L. G. Villanueva, R. B. Karabalin, J.E. Sader, M.L. Roukes, "Control of Nonlinearity in a Doubly-Clamped Nanomechanical Beams", Poster for IEEE International Frequency Control Symposium, San Francisco CA, May (2011).
[2] L. G. Villanueva, R. B. Karabalin, M. H. Matheny, E. Kenig, M.C. Cross, M.L. Roukes, "Nonlinear Dynamics in NEMS", Invited Talk at the International Workshop in NEMS, Toulouse (France), July (2011).*
[3] R. B. Karabalin, M.C. Cross, M.L. Roukes, "Nonlinear Dynamics in NEMS", Invited Talk at ECC-11, Lille (France), July (2010).*

* Associated travel expenses were not charged to any federal grant.

D.4 Book

[1] *Fluctuating Nonlinear Oscillators. From nanomechanics to quantum superconducting circuits"*, ed. M. I. Dykman (OUP, Oxford 2012)

D.5 Theses

[1] N. Miller, Ph.D. dissertation, Department of Mechanical Engineering and Department of Physics and Astronomy, Michigan State University, 2012.
[2] M. Matheny, Ph.D. dissertation, Department of Physics, California Institute of Technology 2013.

ACRONYMS, ABBREVIATIONS, AND SYMBOLS

Acronym	Description
AC	alternating current
AD	Allan Deviation
AFM	atomic force microscopy
AFRL	Air Force Research Laboratory
AlN	aluminum nitride
APN	Anomalous Phase Noise
DARPA	Defense Advanced Research Agency
dB	decibel
DC	direct current
DEFYS	Dynamic Enabled Frequency Sources
FEM	Finite Element Modeling
GHz	gigahertz
KHz	kilohertz
MEMS	Microelectromechanical system
MHz	megahertz
Mo	molybdenum
MSU	Michigan State University
NEMS	nanoelectromechanical system
NF	noise figure
OPO	optical parametric oscillator
PCB	printed circuit board
PFO	periodically forced oscillators
PZE-PZE	Piezoelectric-Piezoelectric
PZE-PZR	Piezoelectric-Piezoresistive
RF	radio frequency
SEM	scanning electron microscope
UHF	ultra-high frequency
VHF	very high frequency